146 (2026) 205827

Contents lists available at ScienceDirect

Gas Science and Engineering

journal homepage: www.journals.elsevier.com/gas-science-and-engineering

Experimental investigation of characteristic frequency of intermittent gas-liquid vertical downward flow

Abderraouf Arabi [a,*], Abdelhak Lakehal [b], Ronaldo Luis Höhn [a], Abdelwahid Azzi [c], Jordi Pallares [a], Youssef Stiriba [a]

[a] Universitat Rovira i Virgili, Departament d'Enginyeria Mecànica, Av. Països Catalans 26, 43007, Tarragona, Spain
[b] Theoretical and Applied Fluid Mechanics Laboratory, Faculty of Physics, University of Science and Technology Houari Boumediene, Bab Ezzouar, Algiers, 16111, Algeria
[c] Laboratoire de Transports Polyphasiques et Milieux Poreux, Faculté de Génie Mécanique et Génie des Procédés, Université des Sciences et de la Technologie Houari Boumédiène, BP 32, El Alia, Bab Ezzouar, Algiers, 16111, Algeria

ARTICLE INFO

Keywords:
Gas-liquid vertical downward flow
Intermittent flow
Characteristic frequency
Flow map
Predictive correlation

ABSTRACT

The estimation and prediction of the characteristic frequency of intermittent structures present in intermittent vertical downward two-phase flow is of primary importance for the design and operations of systems involving this kind of flow. This paper aims to present, for the first time, a detailed quantitative analysis of the characteristic frequencies of intermittent flows in this flow configuration. The study was conducted through a series of experiments in a 30 mm ID pipe using an air–water mixture. Absolute pressure time series were acquired at three axial locations and analyzed using the Welch's method to extract the characteristic frequencies.

Visual observations using a high-speed camera enabled the identification and discussion of the distinct structures present in the three flow regimes (cap bubble, slug and churn) of intermittent flow. Based on an analysis of the forces acting during transitions between the different flow regimes, the dimensionless mixture Froude number and the modified Lockhart–Martinelli parameter were employed for mapping the three flow regimes, demonstrating high predictive capabilities. In addition, the analysis of the measured characteristic frequencies showed that they increase during the flow development, reaching a fully developed value at 56.33 L/D. These frequencies are strongly influenced by the gas superficial velocity. Interestingly, the measured total pressure drops were found to be directly related to both the characteristic frequencies and the flow regime type. Finally, a new empirical correlation was introduced, outperforming the existing one.

Abreviation		
CCS	Carbon capture and storage	
CFD	Computational fluid dynamics	
FFT	Fast Fourier transform	
ID	Inner diameter	
PSD	Power spectral density	
Nomenclature		
a	Empirical coefficient	[-]
AARE	Average absolute relative error	[-]
ARE	Average relative error	[-]
b	Empirical coefficent	[-]
c	Empirical coefficient	[-]
D	Pipe diameter	[m]
$D_{d,max}$	Maximum distorted bubble limit	[m]
dP/dL	Pressure drop gradient	[Pa.m^{-1}]
f_G	Gas friction factor	[-]
f_L	Liquid friction factor	[-]
f_c	Characteristic frequency	[Hz]
$f_{c,\ cal}$	Calculated characteristic frequency	[Hz]
$f_{c,\ mea}$	Measured characteristic frequency	[Hz]
f_s	Slug frequency	[Hz]
Fr_M	Mixture Froude number	[-]
Fr_{SG}	Gas based Froude number	[-]
Fr_{SL}	Liquid based Froude number	[-]
g	Gravitational acceleration	[m.s^{-2}]
Kur	Kurtosis	[-]
L	Length	[m]
N	Number of data points	[-]

(continued on next column)

(continued)

(continued on next page)

* Corresponding author.
E-mail address: abderraouf.arabi@urv.cat (A. Arabi).

https://doi.org/10.1016/j.jgsce.2025.205827
Received 13 June 2025; Received in revised form 10 November 2025; Accepted 14 December 2025
Available online 18 December 2025

(*continued*)

Abreviation		
P	Pressure	[Pa]
P_{max}	Maximum pressure	[Pa]
P_{min}	Minimum pressure	[Pa]
$NFFT$	Number of FFT points used to compute the spectrum	[-]
R^2	Coefficient of determination	[-]
RE	Relative error	[-]
Re_G	Gas Reynolds number	[-]
Re_L	Liquid Reynolds number	[-]
Skw	Skewness	[-]
Std	Standard deviation	[-]
t	Time	[-]
X	Lockhart-Martinelli parameter	[-]
X'	Modified Lockhart-Martinelli parameter	[-]
V_M	Mixture velocity	[m.s^{-1}]
V_{SG}	Gas superficial velocity	[m.s^{-1}]
V_{SL}	Liquid superficial velocity	[m.s^{-1}]
Greek letters		
λ_L	Input liquid fraction	[-]
μ_L	Liquid viscosity	[Pa.s]
ρ_G	Gas density	[kg.m^{-3}]
ρ_L	Liquid density	[kg.m^{-3}]

1. Introduction

Vertical downward gas–liquid two-phase flows are present during the steam and gas injection operations in oil and gas industry as well as in carbon capture and storage (CCS) (Abdulkadir et al., 2021; Hammer et al., 2021; Bai et al., 2023). This latter is widely recognized as a key technology in efforts to mitigate climate change (Vaziri et al., 2024; Bai et al., 2024). This has motivated significant efforts to improve the implementation of CCS projects (Lu et al., 2018; Peng et al., 2024; Chinello et al., 2024), notably through the adaptation of models and software originally developed for multiphase flow in petroleum engineering to CCS applications (Aursand et al., 2013).

Compared to vertical upward flows, the vertical downward two-phase flow has received less attention in the literature. The main studies have primarily focused on flow regimes mapping, or liquid holdup and pressure drop measurements and modeling (Bouyahiaoui et al., 2024). Previous research works (Zadrazil et al., 2014; Qiao et al., 2022; Saidj et al., 2025) have discussed the unique physical phenomena that occur in each vertical downward regime flow, which significantly impact global parameters such as pressure drop and liquid holdup. The reported findings motivate the need for further investigation of the hydrodynamic characteristics of each flow regime, in order to enhance the understanding of flow behavior in this orientation.

Similar to other pipe orientations, vertical downward flows can be categorized into three main regimes: segregated, dispersed, and intermittent (Barnea et al., 1982; Abdul-Majeed et al., 2025). In segregated flow, gas and liquid phases flow separately, as observed in annular and falling film patterns (Ayegba et al., 2025). Dispersed flow involves gas bubbles distributed within a continuous liquid phase (Garbin et al., 2025). Intermittent flow is characterized by alternating sequences of rich liquid and gas structures (Sarkodie et al., 2023; Holagh and Ahmed, 2024; Saidj et al., 2025; Mohmmed et al., 2025). Within vertical downward flows, intermittent regimes include cap bubble, slug, and churn flows.

Intermittent flow is considered the most complex regime from both industrial and modeling perspectives. The alternating presence of the two rich liquid and gas structures can lead to operational challenges such as pipe erosion-corrosion and significant pressure fluctuations (Arabi et al., 2025a). Modeling these flows is further complicated by dynamic interfaces, gas entrainment within liquid slugs, the statistical variability of slug characteristics and the different instabilities present (Fabre and Liné, 1992; Holagh and Ahmed, 2025). Accurate modeling necessitates closure relations for parameters like slug translational velocity, liquid holdup, slug length, and frequency (Arabi et al., 2025a). Therefore, experimental investigations of the hydrodynamics of intermittent flows are essential for developing robust physical models that can predict both flow behavior and associated transport phenomena (Holagh and Ahmed, 2024, 2025; Zhai et al., 2025).

Despite its industrial relevance, vertical downward intermittent flow has been less extensively studied than its upward and horizontal counterparts. The main experimental studies are summarized in Table 1. Martin (1976) and Usui and Sato (1989) examined the complex morphology of Taylor bubble noses in downward flows and their impact on slug translational velocity. Sekoguchi et al. (1996a, 1996b) identified various sub-regimes within slug flow, referred to as plug flows, and highlighted differences in bubble dynamics within liquid slugs across these sub-regimes. Subsequent studies utilized similar experimental setups to analyze liquid slug length distributions and churn flow wave characteristics were carried out by Sekoguchi et al. (1996a) and Mori et al. (1996), respectively. Bouyahiaoui et al. (2018) generated a database of slug parameters from void fraction time series obtained using the conductance probe technique. In a comparative study, Bouyahiaoui et al. (2020) analyzed churn flow behaviors in both upward and downward orientations, revealing differences in distribution coefficients and translational velocities. More recently, Saidj et al. (2025) recently showed differences in slug liquid holdup between upward and downward vertical flows.

On the other hand, the alternating passage of gas and liquid dominant structures in intermittent flow occurs at a natural or intrinsic frequency. Given that intermittent flow is commonly referred to as "slug flow" (Mohmmed et al., 2021), this intrinsic frequency is often termed slug frequency. Throughout this paper, we adopt the broader term intermittent characteristic frequency when referring collectively to cap bubble, slug, and churn flows, while the terms cap bubble frequency, slug frequency, and churn frequency will be used to specify frequency of each regime individually. Slug frequency has garnered significant attention in the literature due to its wide-ranging practical implications. As previously discussed, it serves as a critical closure parameter in one-dimensional mechanistic models used for modelling intermittent flows, which are widely integrated in oil and gas industry simulation tools (Johansson et al., 2024). Recently, Arabi et al. (2025a) emphasized the broader utility of slug frequency in industrial applications. Their

Table 1
Summary of previous experimental investigations focusing on gas-liquid cap bubble, slug and churn flows in vertical downward configuration.

Authors and year	Fluids used	Pipe diameter [mm]	Parameters studied
Martin (1976)	Air-water	26, 101.6 and 140	Slug translational velocity
Usui and Sato (1989)	Air-water	16 and 24	Void fraction profile, and slug translational velocity
Sekoguchi et al. (1996b)	Air-water (at $P = 0.2$ MPa)	25.8	Slug liquid holdup, and gas slug velocity
Sekoguchi et al. (1996a)	Air-water (at $P = 0.2$ MPa)	25.8	Length of liquid slug structures (swelling liquid front zone, and wake zone), and void fraction profile within liquid slug
Mori et al. (1996)	Air-water (at $P = 0.2$ MPa)	25.8	Waves characteristics (time-spatial evolution, width, velocity, and liquid holdup maximal) of churn flow
Bouyahiaoui et al. (2018)	Air-water	34	Slug translational velocity, slug length, Taylor bubble length, liquid film thickness, and slug frequency
Bouyahiaoui et al. (2020)	Air-water	34	Churn translational velocity
Saidj et al. (2025)	Air-water	34	Slug liquid holdup

Table 2
Parameters used in the power density spectral analysis.

Parameter	Value
Time	60 s
Sampling frequency	1000 Hz
Time increment per sample	0.001 s
Window size	2048
Number of ensembles	29
NFFT	65536 (=2^{16})

review showed that slug frequency is not only a modeling tool but also a benchmark for validating three-dimensional computational fluid dynamics (CFD) simulations. Furthermore, this parameter directly affects pressure drop, overall heat transfer coefficient, corrosion rates, and wax deposition in pipelines. In addition, Arabi et al. (2025a) explained that slug frequency affects both the frequency of momentum fluctuations in the pipe, which can trigger resonance phenomena, and the impact forces exerted on pipe fittings. As a result, slug frequency plays a critical role in addressing challenges related to flow-induced vibrations (FIV). This highlights the critical importance of accurately predicting slug frequency, particularly for industries operating with intermittent multiphase flow systems. The inherently complex dynamics governing slug frequency remain insufficiently understood, limiting the effectiveness of purely theoretical models (Mohmmed et al., 2025). As a result, research in this area has predominantly relied on experimental investigations (Gregory and Scott, 1969; Legius et al., 1997; van Hout et al., 2003; Arabi et al., 2020a; Cao et al., 2024; Rodrigues et al., 2025). Consequently, numerous empirical correlations have been proposed to predict slug frequency in horizontal, vertical upward, and inclined pipes (Gregory and Scott, 1969; Heywood and Richardson, 1979; Legius et al., 1997; Fossa et al., 2003; Abdul-Majeed et al., 2020; Arabi et al., 2020; Garcia et al., 2023; Rodrigues et al., 2025).

For vertical downward flow, and to the authors best knowledge, Bouyahiaoui et al. (2018) is the only study in which the measurements of slug frequency in vertical downward flow were carried out. The authors proposed an empirical correlation for predicting the slug frequency (f_s), given as:

$$f_s = 0.1014\lambda_L\left(\frac{0.0117}{D}+\frac{V_M^2}{gD}\right) \tag{1}$$

where D, g, V_M and λ_L are the pipe diameter, gravitational acceleration, mixture velocity, and input liquid fraction, respectively. The mixture velocity corresponds to the sum of the liquid and gas superficial velocities (Eq. (2)), while the input liquid fraction refers to the liquid holdup in the case of no slip between the two phases (Eq. (3)).

$$V_M = V_{SL} + V_{SG} \tag{2}$$

$$\lambda_L = \frac{V_{SL}}{V_M} \tag{3}$$

An analysis of the work by Bouyahiaoui et al. (2018) shows that the authors did not perform a parametric study on the factors influencing slug frequency. This indicates that slug frequency remains largely underexplored in vertical downward flow. This knowledge gap is even more pronounced in the case of cap bubble and churn flow frequencies, which have received no attention in the literature.

From the presented state-of-the-art, it can be concluded that advancing the understanding of intermittent vertical downward flow requires a detailed characterization of its characteristic frequencies, which have received limited attention in the previous studies. The present study aims to fill this gap through a comprehensive experimental analysis of the characteristic frequencies associated with cap-bubble, slug, and churn flows. The influence of gas superficial velocity and the spatial evolution of these frequencies are analyzed for the first time in this flow orientation. Additionally, the relationship between these frequencies and the overall pressure drop is examined, and a new empirical correlation is finally proposed.

2. Experimental setup and data processing

2.1. Experimental facility

The schematic diagram of the experimental facility used in this study is presented in Fig. 1. The test section is constructed from transparent acrylic and has an inner diameter of 30 mm. It is composed of four distinct sections: a bottom horizontal segment, a vertical upward segment, a top horizontal segment, and a vertical downward segment, with respective lengths of 5.10 m, 3.36 m, 5.10 m and 3.00 m. These segments are interconnected by bends with a radius of curvature of 219.9 mm. A centrifugal pump circulates water from a storage tank to the inlet mixer, and the liquid flow rate is regulated via a variable frequency drive (VFD). Flow rate measurements are performed using an electromagnetic flow meter with an accuracy of ±0.8 %. The gas mass flow rate is controlled and monitored by a mass flow controller with a precision of ±0.8 %. Air and water phases are mixed using a Y-type mixer, where the water is injected horizontally at the entrance of the bottom horizontal section. For additional details about the experimental setup, readers are referred to our previous works (Sassi et al., 2022; Höhn et al., 2025). The maximum absolute uncertainties associated with the liquid and gas superficial velocities are estimated to be 0.02 m/s and 0.05 m/s, respectively. Further details are provided in Arabi et al. (2025b).

2.2. Instrumentation

The absolute pressure time series were recorded using Omega PX482A-060AI transducers located in vertical downward flow section, which offer an accuracy of ±0.3 %. The transducers were installed at three axial positions corresponding to $L/D = 23.00$, $L/D = 56.33$, and $L/D = 73.00$, where L is the distance from the end of the 90° bend. Pressure time series data were simultaneously acquired using a Keysight U2542A USB data acquisition system, operating at a sampling frequency of 1000 Hz over a duration of 60 s. Flow visualization was carried out using a Photron FASTCAM Mini UX100 high-speed camera (800K type), and positioned approximately at $L/D \approx 87.00$.

2.3. Pressure time series processing

In this study, the characteristic frequencies were obtained from pressure time series recorded using absolute pressure transducers, described in Section 2.1. This instrumentation is notable for its robustness, non-intrusive nature, ease of implementation, and industrial applicability (Arabi et al., 2024). Given that this type of sensor is widely used across various scales, the results obtained at the laboratory scale can be reliably extrapolated to semi-pilot, pilot, and industrial scales. As shown in the flowchart depicted in Fig. 2, the collected pressure time series are first filtered before applying Power Spectral Density (PSD) analysis to extract the characteristic frequency. Each step is further explained below:

a Raw data filtering

The raw parietal pressure time series were denoised using a wavelet-based filtering approach. Specifically, the Daubechies wavelet method (Daubechies, 1992) was employed, utilizing the MATLAB code developed by Soto-Cortés et al. (2021a, 2021b). This algorithm relies on a Symlet4 wave decomposition, which has been shown by Soto-Cortes (2014) to be particularly suitable for analyzing "slug-like" signals. Given that the optimal filtering level depends on the noise content of the signal (Soedarmo et al., 2019), a sensitivity analysis was performed using multiple filter levels (1 through 5). As illustrated in Fig. 3, based on a

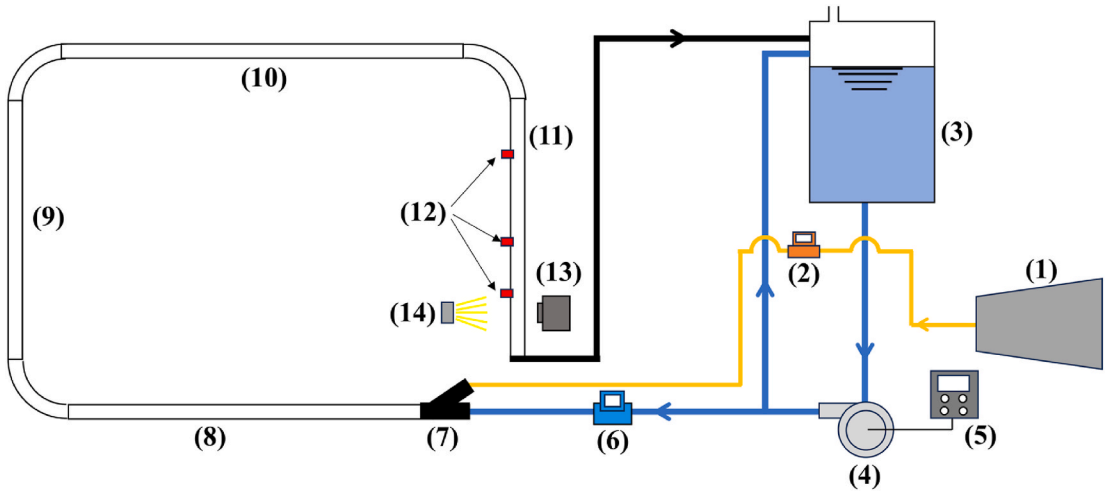

Fig. 1. Schematic diagram of experimental setup used in the present study. (1) air compressor; (2) gas mass flowmeter; (3) water tank; (4) water pump; (5) VFD; (6) liquid flowmeter; (7) air-water inlet mixer; (8) bottom horizontal segment; (9) vertical upward segment; (10) top horizontal segment; (11) vertical downward segment; (12) pressure transducers; (13) high-speed camera; and (14) LED projector.

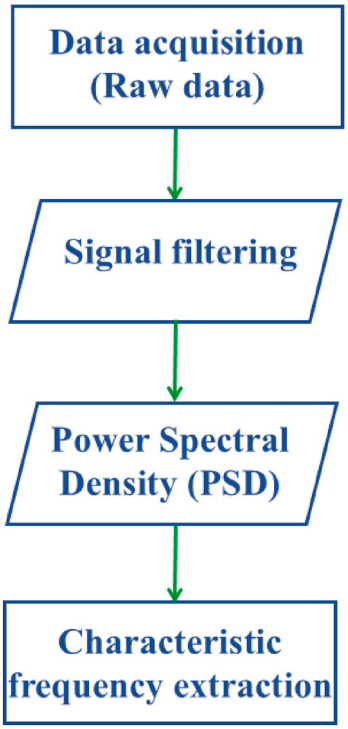

Fig. 2. Flowchart of the pressure signal processing procedure adopted in the present study. Rectangles represent input and outputs, while parallelograms denote signal processing steps.

representative signal collected at $V_{SL} = 2.05$ m/s and $V_{SG} = 3.00$ m/s, no significant change in the filtered signal was observed beyond level 3. By plotting the evolution of key statistical parameters including, maximum pressure (P_{max}), minimum pressure (P_{min}), standard deviation (*Std*), skewness (*Skw*), and kurtosis (*Kur*), against the filter level in Fig. 4, it was observed that all parameters reach asymptotic values at level 3. Following the recommendation of Soedarmo et al. (2019), the lowest filtering level beyond which no substantial signal alteration occurs was selected. Thus, the filter level 3 was adopted for all subsequent data processing.

b Power spectral density

The Fast Fourier Transform (FFT) is a computationally efficient method widely used to estimate the frequency content of time series data. It has been described as "the most important numerical algorithm of our lifetime" (Henry, 2024). In the context of multiphase flow, FFT is typically employed to analyze the energy distribution within a signal via the power spectral density function.

In the present study, we applied the Welch's method, implemented through the function pwelch in MATLAB, to extract the frequency components from the mean-centered pressure fluctuation time series. The parameters used in the PSD analysis are summarized in Table 2. Readers interested in further details of the methodology are referred to Soto-Cortès et al. (2021a, 2021b) and Al-Alweet et al. (2025). The choice of the Welch method is motivated by its use of smoothing techniques, which enhance the resolution of spectral peaks and reduce noise, resulting in clearer identification of dominant frequencies. This benefit, highlighted by Schmelter et al. (2021), is clearly illustrated in Fig. 5., which compare typical frequency spectra obtained using the Welch's method and the classical FFT, respectively. In these spectra, the dominant frequency, identified by the highest amplitude peak, corresponds to the main structure frequency present in the flow. Smaller secondary peaks are attributed to the presence of harmonic frequencies (Hernandez–Perez et al., 2010a). The dominant frequency is often referred in the literature to the characteristic frequency of the flow (Hernandez–Perez et al., 2010a; Arabi et al., 2020). The extraction of dominant frequency from the PSD spectrum has been employed in numerous studies, as recently detailed in the review on slug frequency measurement presented by Höhn et al. (2024).

2.4. Test matrix

A total of 50 experimental conditions were selected for the present study. The experiments were conducted using four distinct liquid superficial velocities of 1.75, 2.05, 2.36, and 2.63 m/s, combined with thirteen gas superficial velocities ranging from 0.20 to 6.00 m/s. The complete experimental matrix is illustrated in Fig. 6. Due to limitations of the present experimental setup, particularly the capacity of the pumping system, it was not possible to achieve V_{SG} values exceeding 4 m/s for $V_{SL} = 2.63$ m/s. For comparative purposes, the experimental conditions from the study of Bouyahiaoui et al. (2018) are also included in Fig. 6. It is noteworthy that the present study explores a greater values of V_{SL} compared to the work of Bouyahiaoui et al. (2018). The narrower range of V_{SG} in their experiments can be attributed to their exclusive focus on slug flow regimes.

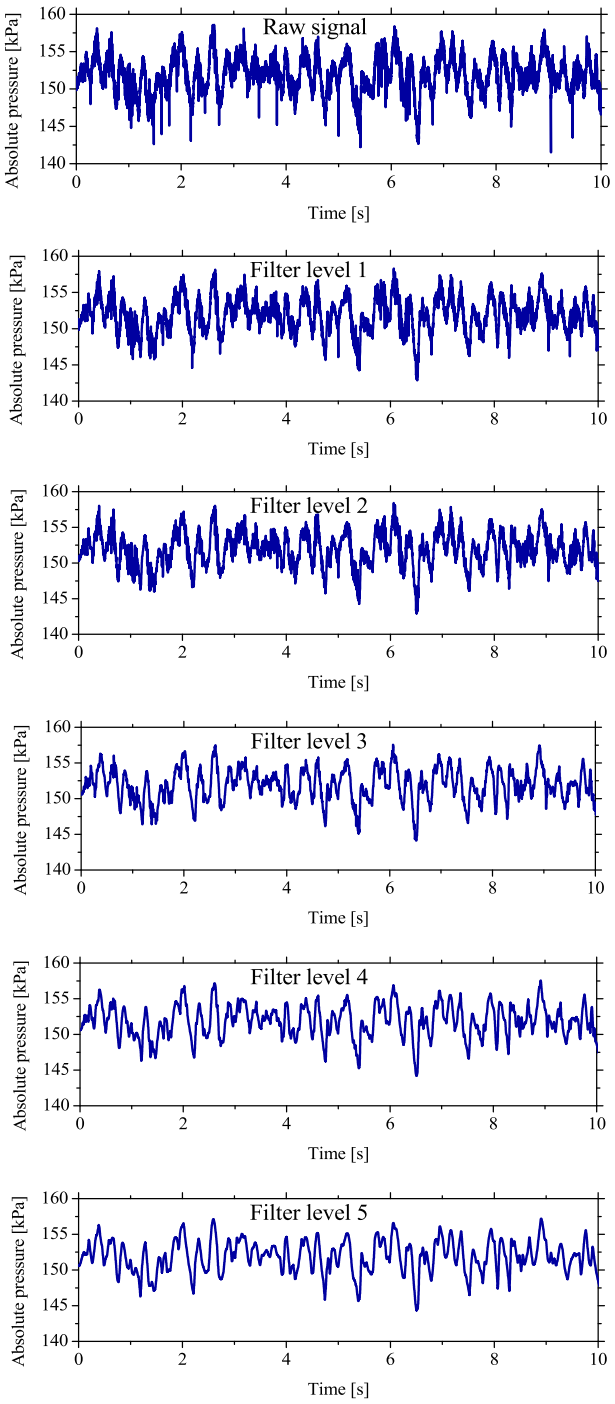

Fig. 3. Example of data filtering results collected for $V_{SL} = 2.05$ m/s and $V_{SG} = 3.00$ m/s at $L/D = 73.00$.

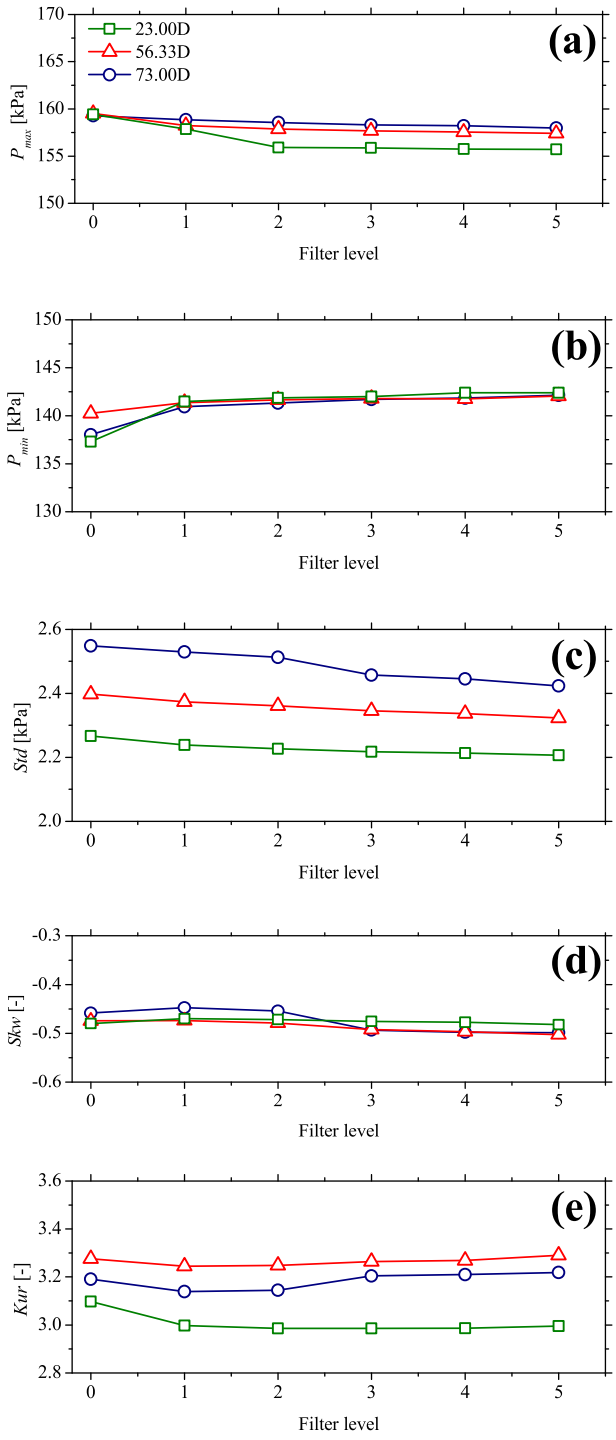

Fig. 4. Evolution of (a) maximum absolute pressure (P_{max}), (b) minimum absolute pressure (P_{min}), (c) standard deviation (*Std*), (d) skewness (*Skw*) and (e) kurtosis (*kur*) as function of the filtered level for $V_{SL} = 2.05$ m/s and $V_{SG} = 3.00$ m/s at different axis locations. The filter level 0 corresponds to the raw signals.

3. Results and discussion

3.1. Flow regimes

Fig. 7 presents a sequence of images illustrating the flow structures observed under cap bubble flow conditions at $V_{SL} = 2.63$ m/s and $V_{SG} = 0.25$ m/s. The flow consists of a continuous liquid phase within which gas is transported in the form of two different length classes of bubbles: small scall dispersed bubbles and larger scale cap-shaped bubbles. The characteristic length of the cap bubbles is of the same order of magnitude as the pipe diameter, and, as consequence, exceeds the maximum stable diameter of distorted bubbles ($D_{d,\,max}$) as defined in Eq. (4) (Ishii and Zuber, 1979). According to this criterion, these structures are qualified as Group II bubbles (Hibiki et al., 2004). Consequently, the cap bubble flow regime has to be categorized as an intermittent flow rather than bubbly flow. It is worth noting that Sekoguchi et al. (1996b) previously described cap bubble flow as a sub-regime of slug flow, referring to it under the abbreviation P_{LU}.

$$D_{d,max} = 4\sqrt{\frac{\sigma}{g(\rho_L - \rho_G)}} \tag{4}$$

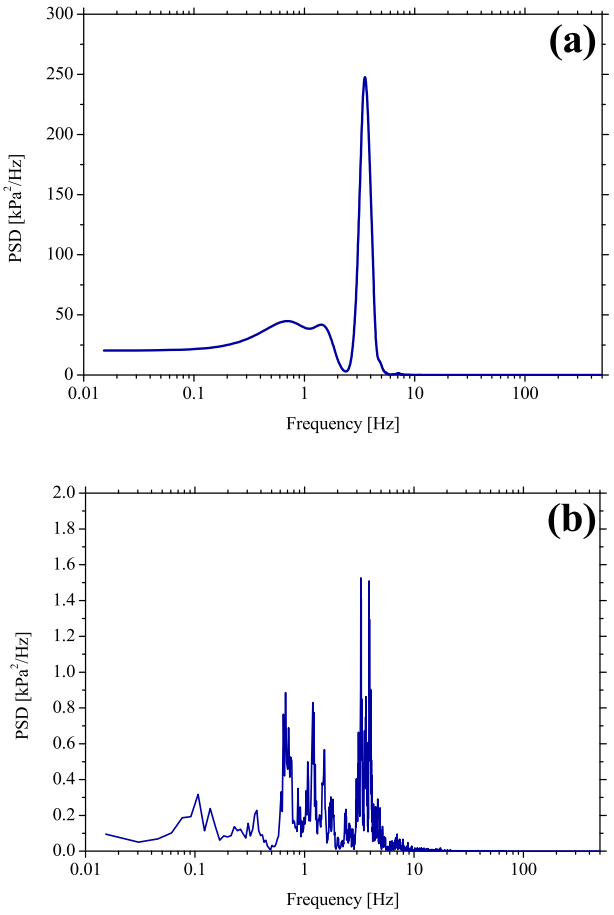

Fig. 5. Example of PSD obtained using (a) Welch method and (b) classical PSD (V_{SL} = 2.05 m/s and V_{SG} = 3.00 m/s at 73.00D).

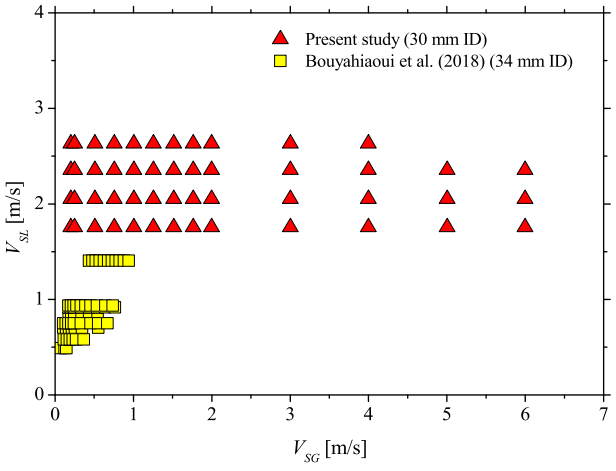

Fig. 6. Plot of the experimental conditions of the present study as well as those of Bouyahiaoui et al. (2018) in a V_{SL} vs V_{SG} chart.

Cap bubbles arise as a result of bubble coalescence, which intensifies with the increase in void fraction driven by the rising gas superficial velocity. In vertical downward flow, dispersed gas bubbles tend to concentrate toward the center of the pipe (Qiao et al., 2022). As a result, the coalescence rate in this configuration is higher than that observed in vertical upward flow. Given their larger volume and the influence of buoyancy, cap bubbles generally travel at a lower velocity than dispersed bubbles. This difference of velocity leads to frequent collisions and coalescence between dispersed and cap bubbles. These interactions predominantly occur in the upper region of the cap bubbles, as clearly illustrated in the image sequence captured between 37.5 ms and 62.50 ms (Fig. 7.g-k).

As the gas flow rate increases, the frequency and intensity of bubbles interactions rise accordingly, promoting the progressive coalescence into elongated gas bubbles known as Taylor bubbles, named in honor of Geoffrey Taylor, the British physicist and mathematician renowned for his pioneering work on slug flow. These bubbles are hallmark features of slug flow. In this regime, the flow is characterized by a distinct alternation between Taylor bubbles encased in an annular liquid film and liquid slugs transporting dispersed gas bubbles. Representative images of these structures observed are shown in Fig. 8. Similar to vertical upward flow, the elongated bubble in vertical downward flow displays a rounded nose and a relatively flat tail pointing upward. Moreover, the elongated bubble exhibits a more irregular interface than that typically observed in vertical upward slug flow. A region of intense turbulence is can typically be seen at the interface between the elongated bubble and the preceding liquid slug, which is refereed as wake region. This turbulence stems from the recirculating zone formed by the plunging liquid jet, which develops as the surrounding annular film converges and impacts the bubble's tail. This plunging jet is induced by the momentum of the trailing liquid slug exerting pressure on the Taylor bubble, as recently described by Saidj et al. (2025).

Interestingly, for V_{SL} = 2.63 m/s and low gas superficial velocities, the elongated bubble adopts a distinct morphology compared to other conditions. As depicted in Fig. 9, both the nose and tail of the bubble appear rounded, giving it a more symmetrical shape. To the best of the authors' knowledge, this flow behavior was only previously discussed by Sekoguchi et al. (1996a, 1996b), who categorized it as P_{LS} flow. In this sub-regime, they also reported a reduced slippage velocity between the gas bubbles and the surrounding liquid within the slugs.

As observed in vertical upward flow, further increases in the gas superficial velocity leads to the breakdown of the interface between elongated gas bubbles and liquid slugs, resulting in the transition to churn flow. Representative images of churn flow captured at V_{SL} = 2.63 m/s and V_{SG} = 4.00 m/s are presented in Fig. 10. In this regime, the previously well-defined Taylor bubbles are replaced by wisps, gas pathways meandering through liquid-rich zones. These structures are analogous to those observed in vertical upward churn flow, as described in Hernandez-Perez et al. (2010b). Within the wisps, disturbance waves (surrounded in yellow in Fig. 10.a-f) can be observed propagating through the gas-liquid mixture (Fig. 10.a-h). Following the wisps, one can see a highly aerated liquid bridge transporting a significant number of small gas bubbles (Fig. 10.i). This bridge, characterized by its intense gas entrainment and chaotic motion, contributes to the pulsating and unstable nature typical of churn flow.

3.2. Flow regime map

To date, identifying the most appropriate coordinates systems for flow regime mapping remains a challenge (Wu et al., 2017; Arellano et al., 2020; Osundare et al., 2022; Korelstein and Pereyra, 2023; Arabi et al., 2025c). The observed flow regimes result from the interplay of various forces acting within the two-phase system. In vertical downward flow, a key factor is the competition between the gas-liquid mixture inertial force and the buoyancy force, which acts in the direction opposite to the flow. This force balance can be characterized by the mixture Froude number (Fr_M) defined in Eq. (5).

$$Fr_M = \sqrt{\frac{\rho_L}{(\rho_L - \rho_G)}}\ \frac{V_M}{\sqrt{gD}} \tag{5}$$

On the other hand, in vertical downward flow, the gas–liquid mixture is also subject to a competing interaction between the inertia of the gas and liquid phases. This balance can be effectively characterized

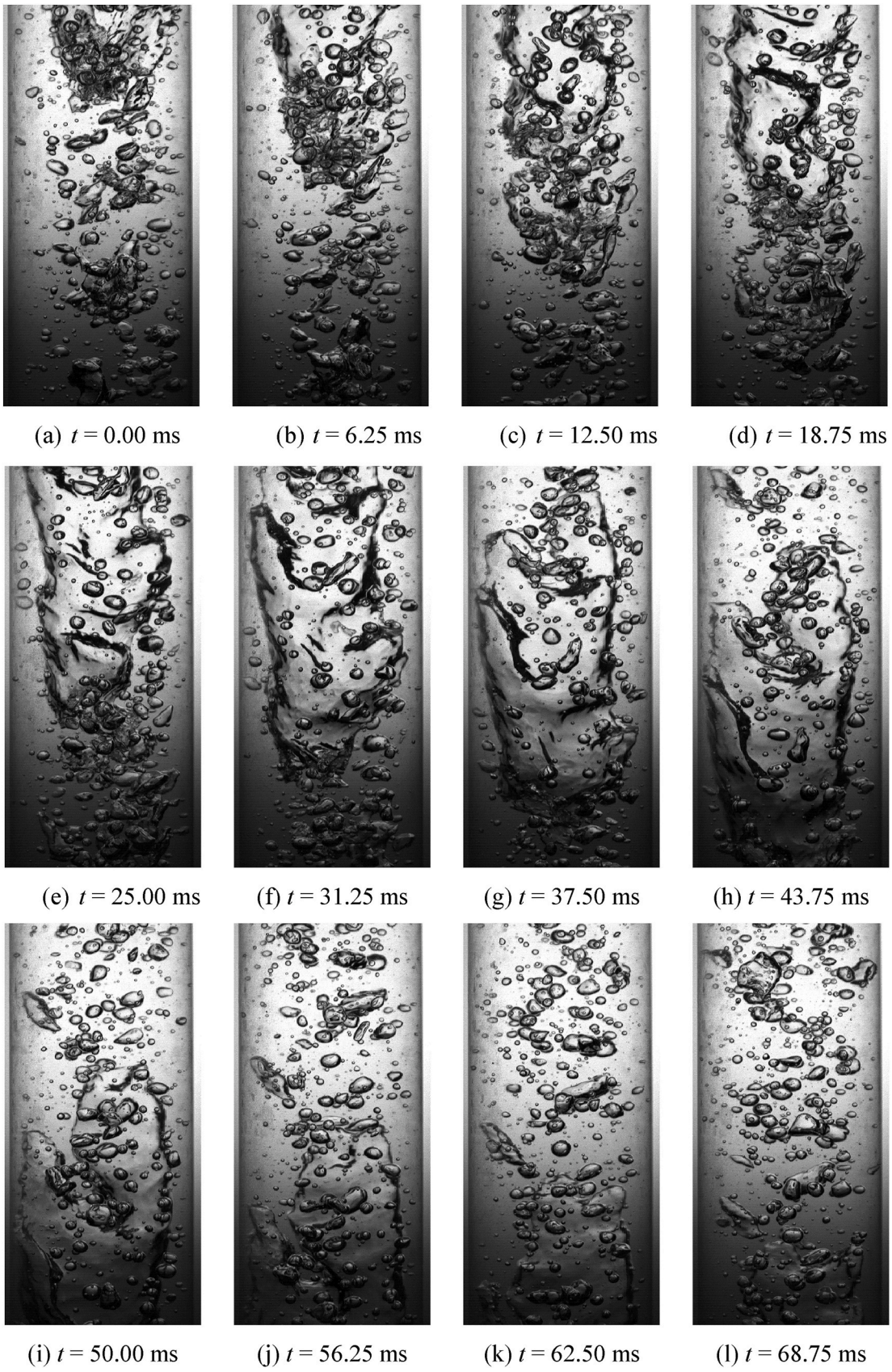

Fig. 7. Successive images of flow structures present in cap bubble flow observed at V_{SL} = 2.63 m/s and V_{SG} = 0.25 m/s.

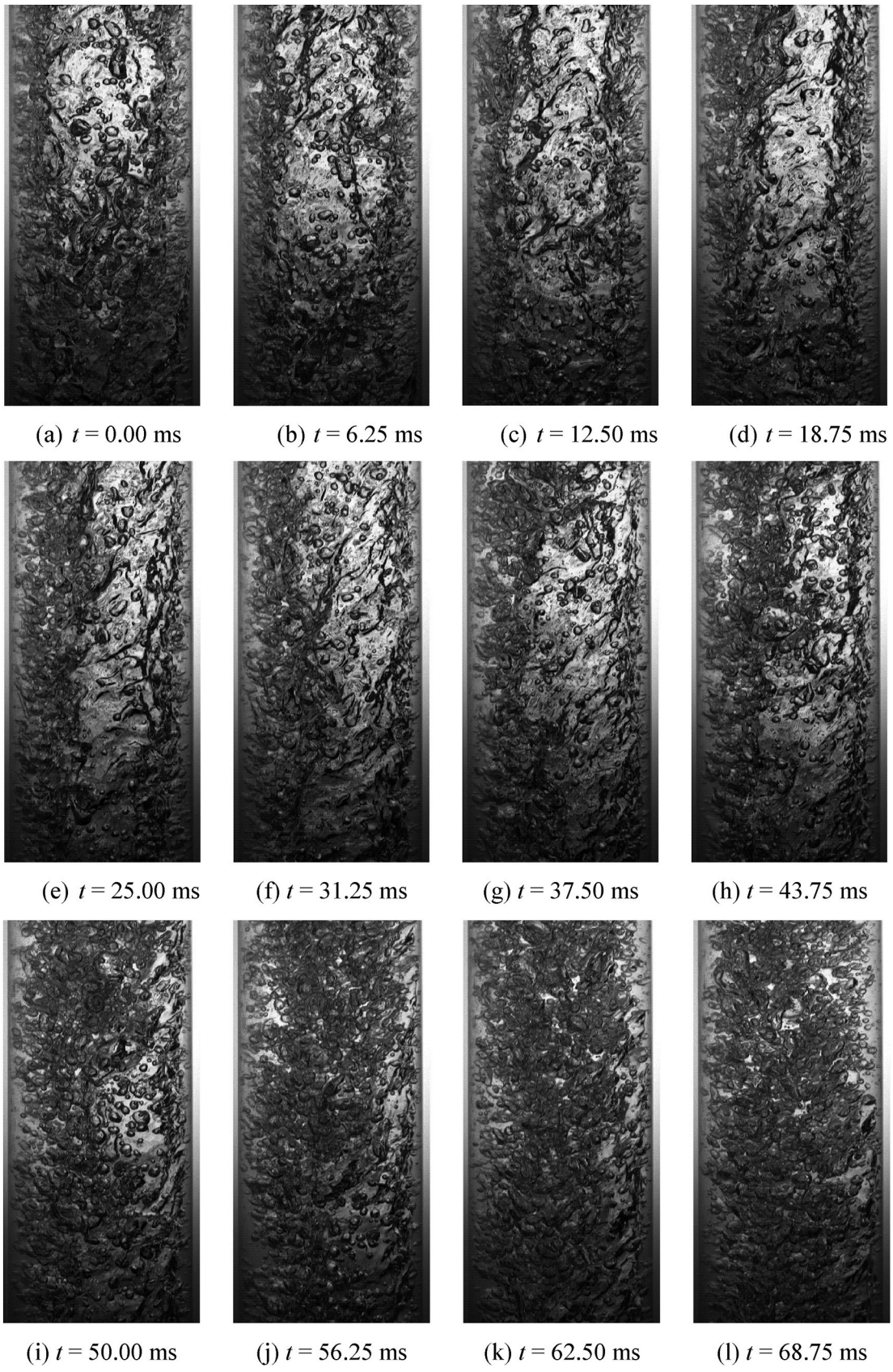

Fig. 8. Successive images of flow structures present in slug flow observed at V_{SL} = 2.63 m/s and V_{SG} = 1.51 m/s.

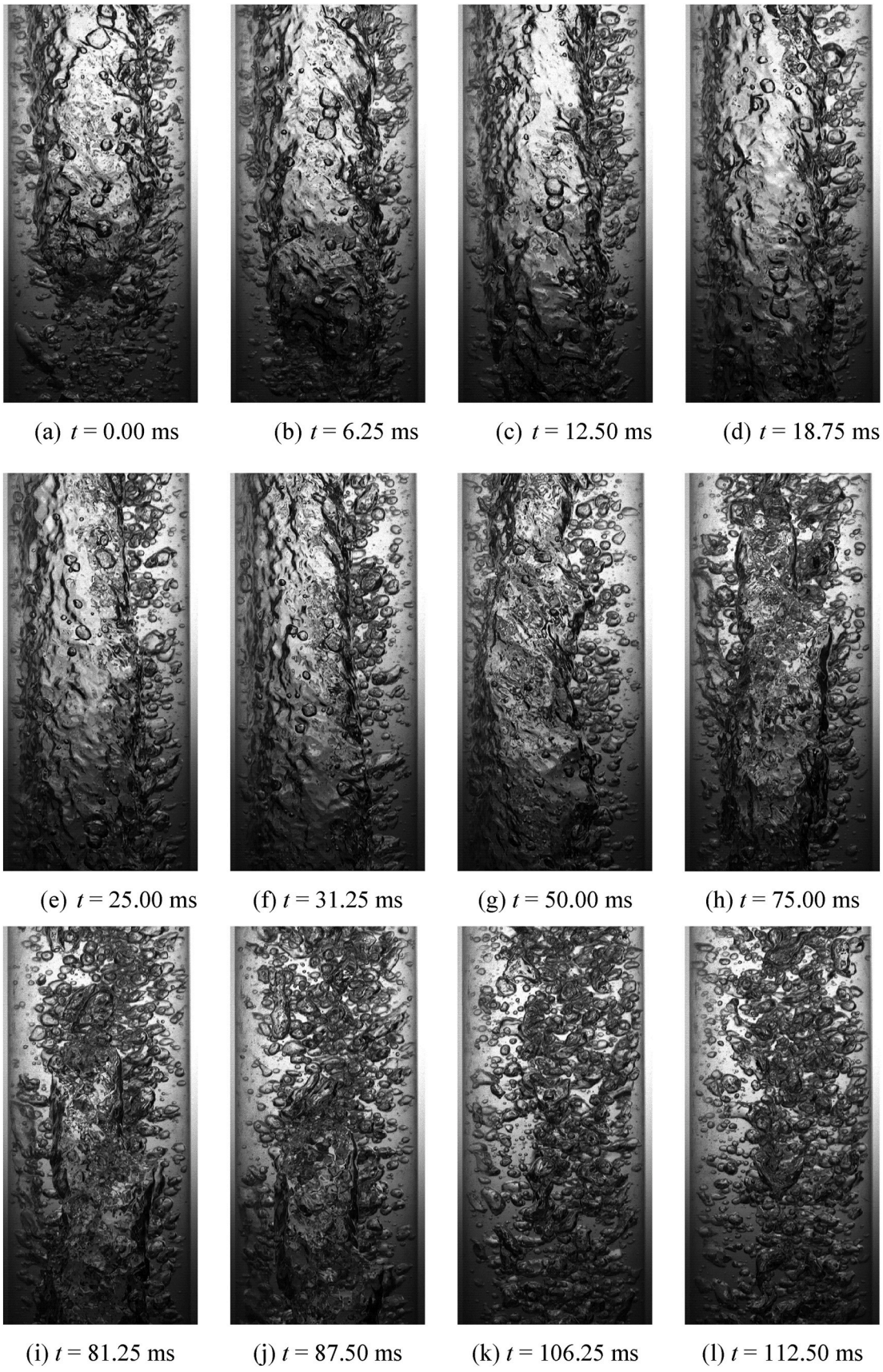

Fig. 9. Successive images of flow structures present in slug flow (P_{LS}) observed at V_{SL} = 2.63 m/s and V_{SG} = 0.76 m/s.

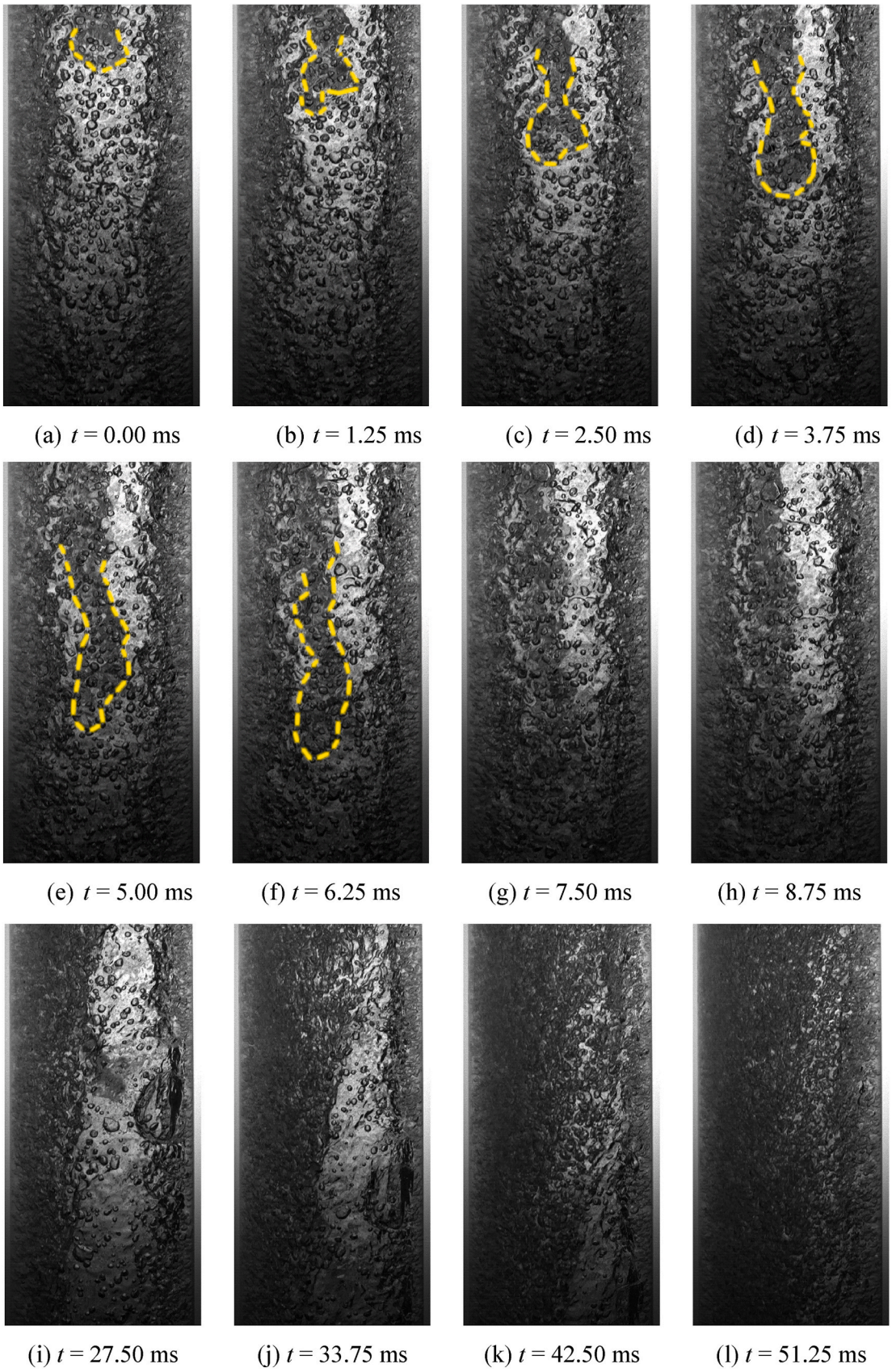

Fig. 10. Successive images of flow structures present in churn flow observed at V_{SL} = 2.63 m/s and V_{SG} = 4.00 m/s.

using the modified Lockhart-Martinelli parameter (X'), which represents the ratio of the liquid-based Froude number (Fr_{SL}) to the gas-based Froude number (Fr_{SG}), as shown in Eq. (6).

$$X' = \frac{Fr_{SL}}{Fr_{SG}} = \frac{\sqrt{\frac{\rho_L}{(\rho_L-\rho_G)}}\ \frac{V_{SL}}{\sqrt{gD}}}{\sqrt{\frac{\rho_G}{(\rho_L-\rho_G)}}\ \frac{V_{SG}}{\sqrt{gD}}} = \sqrt{\frac{\rho_L}{\rho_G}}\ \frac{V_{SL}}{V_{SG}} \tag{6}$$

Based on this analysis, the present experimental conditions as well as those of Lee et al. (2008), Lu et al. (2018) and Bouyahiaoui et al. (2024) corresponding to the three studied flow regimes were plotted on a flow map using the modified Lockhart–Martinelli parameter and the mixture Froude number as coordinates in Fig. 11. The resulting flow map clearly illustrates that the cap bubble, slug, and churn flow regimes observed for different pipe diameters occupy distinct and separate regions, thereby demonstrating the effectiveness of the X' vs Fr_M coordinates system in delineating flow regime boundaries for vertical downward gas–liquid flows. The cap bubble-to-slug and slug-to-churn flow transitions occur at approximate X' values of 165 and 40, respectively. The performance of the proposed flow map was evaluated by calculating the prediction success rate (in %), defined as the ratio between the number of correctly predicted flow regime occurrences and the total number of experimental data points, for each flow regime and each dataset. This method was notably employed by Pereyra et al. (2012), and more recently by Boutaghane et al. (2023) and Arabi et al. (2025c). The results, summarized in Table 3, clearly show that the success rate exceeds 80 % in the vast majority of cases, which can be considered a good level of prediction accuracy according to Boutaghane et al. (2023).

3.3. Pressure time series

Fig. 12 shows representative examples of wall pressure fluctuations measured by the third pressure transducer, located at $L/D = 73.00$, for the three flow regimes investigated. To better emphasize peak dynamics and facilitate comparison across the regimes, only a 10 s portion of the pressure time series is displayed for each case. The signals were mean-centered to eliminate bias from the average pressure value, and a distinct color was assigned to each flow regime for clarity. In all cases, the time series exhibit alternating peaks and valleys, characteristic of the intermittent nature of cap bubble, slug, and churn flows. These fluctuations result from variations of the liquid holdup and shear stress, which in turn impact the local absolute pressure. A clear trend is observed: for a given liquid superficial velocity, the transition from cap bubble to slug flow, and subsequently to churn flow, is accompanied by a successive increase in peak amplitude.

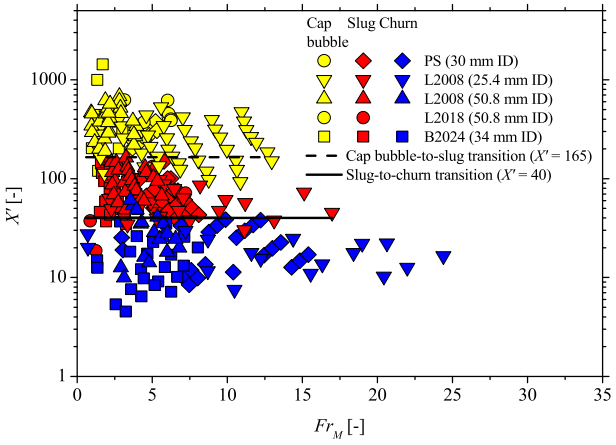

Fig. 11. Plot of observed flow regimes in the present and by several authors in the flow chart using X' vs FrM coordinates. The abbreviations PS, L2008, L2018 and B2024 refer for present study, Lee et al. (2008), Lu et al. (2018) and Bouyahiaoui et al. (2024), respectively.

Table 3
Prediction successful rate of the proposed flow map.

Database	Pipe diameter [mm]	Flow regime	Number of points	Successful rate (%)
Lee et al. (2008)	25.4	Cap bubble[a]	50	70.00
		Slug	27	81.48
		Churn	17	100.00
Lee et al. (2008)	50.8	Cap bubble[a]	28	100.00
		Slug	25	100.00
		Churn	20	80.00
Lu et al. (2018)	50.8	Cap bubble[b]	10	100.00
		Slug	4	50.00
Bouyahiaoui et al. (2024)	34	Cap bubble	8	87.50
		Slug	27	85.19
		Churn	23	100.00
Present study	30	Cap bubble	8	100.00
		Slug	20	95.00
		Churn	22	100.00

[a] The terminology “cap bubbly flow” was used to refer to cap bubble flow in this reference.
[b] The terminology “transitional flow” was used to refer to cap bubble flow in this reference.

The closer inspection reveals that the signals contain multiple scales of pressure peaks. This observation is consistent with the inherently multi-scale nature of intermittent two-phase flow. As notably discussed in Section 3.1, intermittent flow comprises a variety of interacting structures, including turbulent eddies in the liquid phase, dispersed gas bubbles within liquid slugs, wake regions with recirculation, and gas–liquid interfaces surrounding cap and elongated bubbles (Cavalli et al., 2024). In churn flow, this complexity is further amplified by the presence of large disturbance waves, wisps and highly aerated liquid bridges. Due to the wall pressure signal’s sensitivity to hydrodynamic interactions at different spatial and temporal scales, it becomes extremely difficult to isolate and count individual peaks corresponding to elongated bubble or liquid slug passages. Consequently, the direct extraction of characteristic frequency from peak analysis is impractical, thereby justifying the use of a frequency-domain method for accurate quantification. Similar observation was made by Akhlaghi et al. (2020) in their investigation on horizontal pipe.

3.4. Characteristic frequencies

Fig. 13.a presents representative PSD spectra obtained at various axial positions along the vertical downward test section. At the upstream location (=23 L/D), the PSD exhibits a bimodal distribution, with a pronounced secondary peak. As the flow progresses downstream, this secondary peak gradually diminishes, while the amplitude of the primary peak increases. The corresponding characteristic frequencies (f_c) extracted at different axial positions are plotted in Fig. 13.b for the three investigated flow regimes (cap bubble, slug, and churn flows). A clear trend emerges: the characteristic frequency generally increases with axial distance, suggesting that flow development in vertical downward orientation is accompanied by a fragmentation of the intermittent structures. This behavior contrasts with that observed in horizontal and vertical upward flows, where flow development typically leads to a decrease in frequency due to slug coalescence and growth (Waltrich et al., 2013; Kong and Kim, 2021). In the case of slug flow, this phenomenon can be attributed to the difference between the liquid slug velocity and the Taylor bubble translational velocity. In vertical downward flow, the latter is lower than the liquid slug velocity, leading to the formation of a draining liquid film around the bubble periphery. This film results in a plunging jet at the bubble base, which promotes the

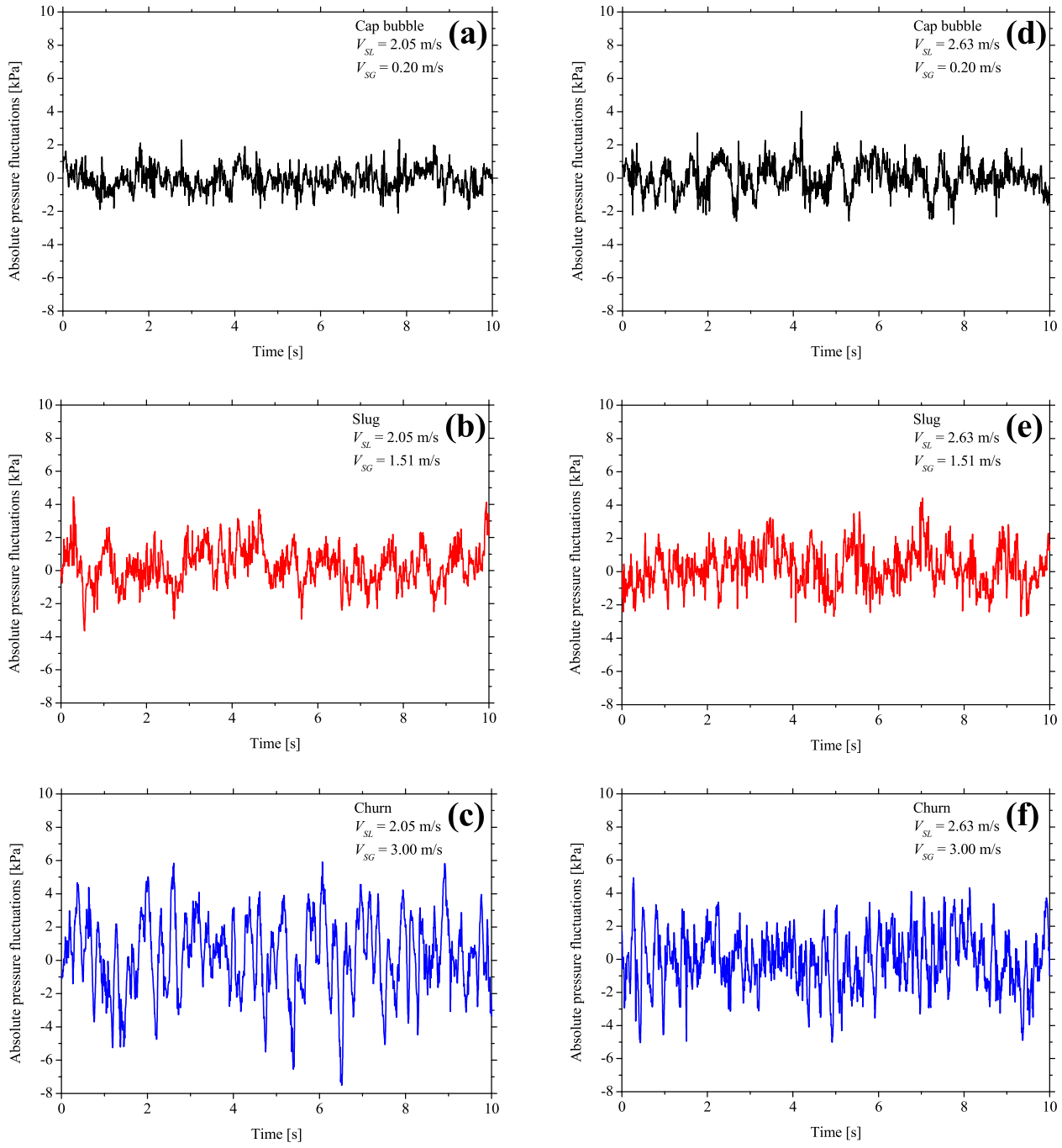

Fig. 12. Examples of signals collected of the three flow regimes studied for different conditions of gas and liquid superficial velocities.

detachment of gas bubbles from the elongated structure in the wake region (Saidj et al., 2025). These detached bubbles may subsequently coalesce forming new Taylor bubbles, which increases the slug frequency along the pipe. However, this hypothesis requires further validation through advanced imaging techniques, such as tomographic flow visualization, placed at multiple axial positions.

Additionally, Fig. 13.b indicates that the characteristic frequency reaches an asymptotic value beyond the second measurement location, suggesting the onset of fully developed flow conditions. This observation is further validated by cross-plotting the cap bubble, slug, and churn frequencies measured at 73.00D and 56.33D (Fig. 13.c), where the majority of the data points exhibit a relative difference within ±10 %. This level of agreement can be considered highly satisfactory given the inherent variability associated with intermittent flow frequency measurements (Höhn et al., 2024).

Fig. 14 presents the evolution of the characteristic frequencies extracted from the PSD as a function of gas superficial velocity at $L = 73.00D$, for various values of V_{SL}. From this figure, it is evident that increasing V_{SG} leads to a rise in cap bubble frequency. The transition from cap bubble to slug flow is marked by a sudden drop in characteristic frequency, which can be attributed to the formation of significantly longer gas structures, Taylor bubbles, during this regime change. The elongation of bubbles reduces their passing frequency, hence the observed drop. For slug flow, a general trend of increasing frequency with rising V_{SG} is observed, though the general increment is modest. This positive correlation can be explained by the increase in slug translational velocity as gas flow rate increases, leading to a higher frequency of slug passage. It is worth noting that for $V_{SL} = 2.63$ m/s and 0.51 m/s

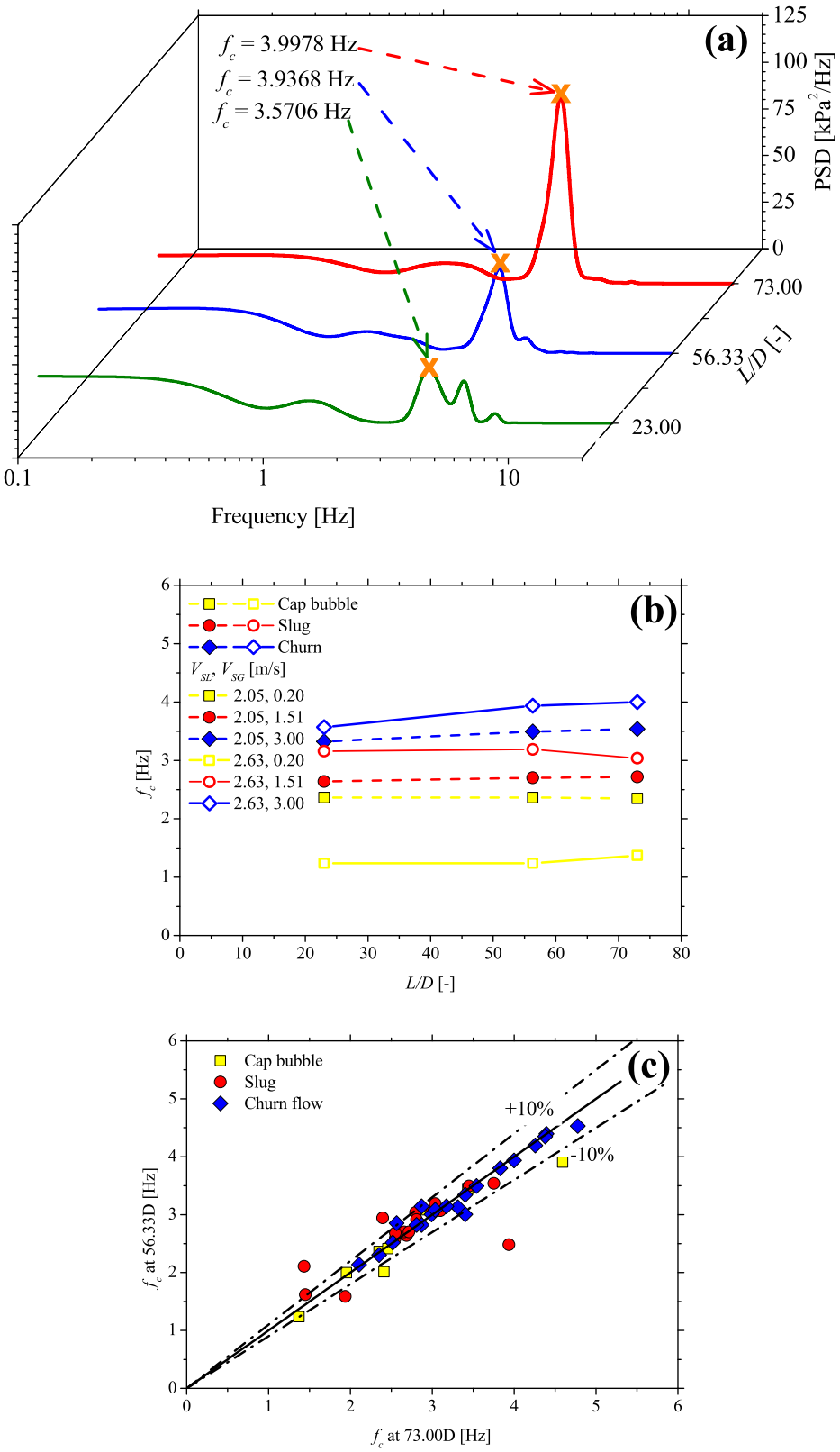

Fig. 13. (a)Variation of PSD along the axial location for V_{SL} = 2.63 m/s and V_{SG} = 3.00 m/s; (b) variation of the dominant frequencies along the axial locations for different experimental conditions; and (c) comparison between the collected characteristic frequencies at 73.00D and 56.33 D.

$\leq V_{SG} \leq$ 1.01 m/s, as shown in Fig. 14.d, the slug frequency ranges between 1.32 and 1.45 Hz, which is significantly lower than the other slug frequency values recorded at the same liquid superficial velocity. Interestingly, these conditions correspond to the cases where the P_{LS} sub-regime was observed.

In the churn flow regime, a non-monotonic behavior of frequency with increasing V_{SG} is observed for each V_{SL}: (i) an initial rise in churn frequency with V_{SG}, (ii) a peak followed by a decline; and (iii) a

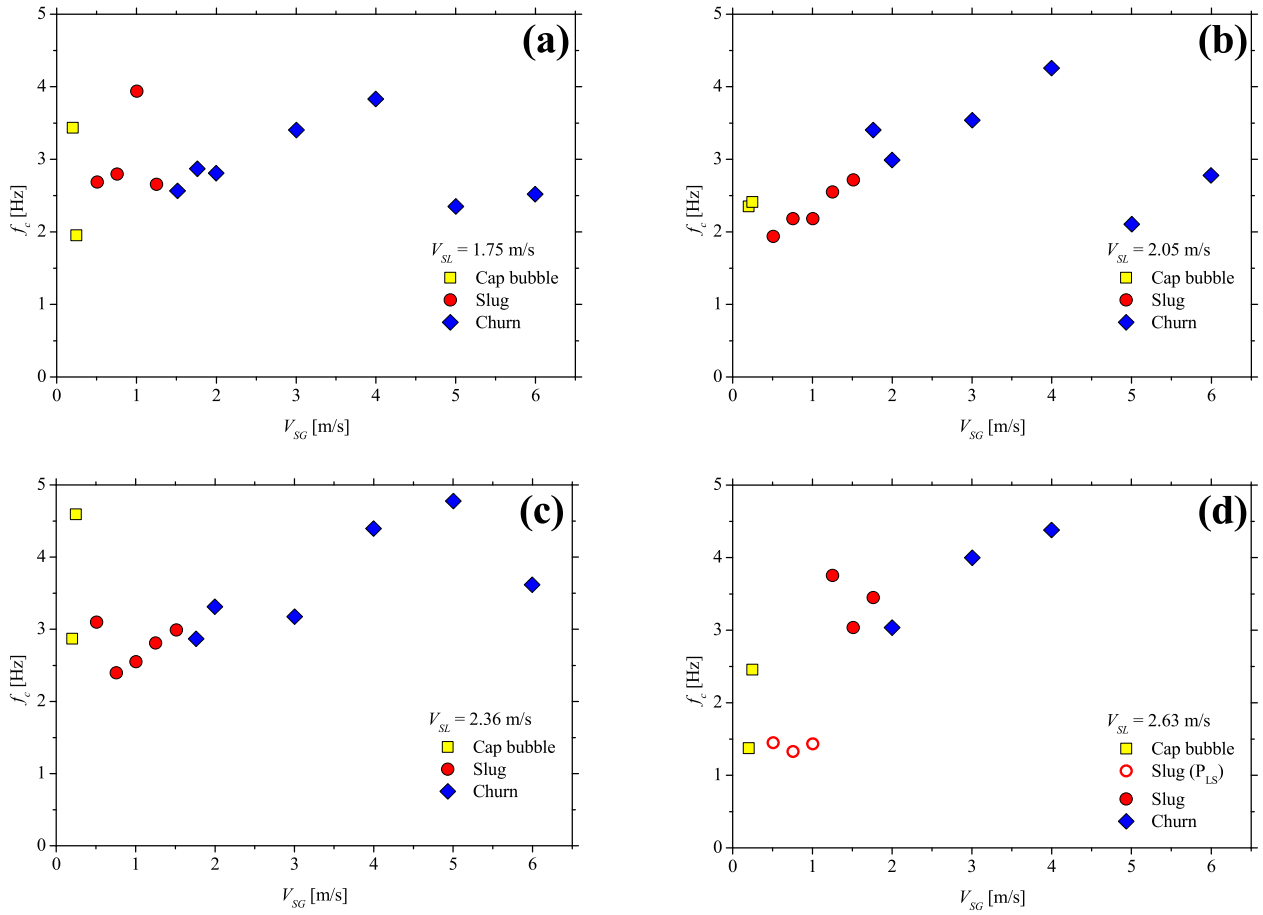

Fig. 14. Influence of V_{SG} on characteristic frequencies for different V_{SL}.

secondary increase at higher V_{SG}. This complex trend is a reflection of the multiscale and chaotic nature of churn flow, characterized by the simultaneous presence of disturbance waves, wisps, and liquid bridges, each potentially contributing to different frequency components. Since the PSD analysis yields only the dominant frequency, it may correspond to the oscillations of one specific structure or an amalgam of overlapping signals. Further experimental investigations aimed at measuring the characteristic frequencies of each flow structure, similar to the work of Sekoguchi and Mori (1997) conducted for vertical upward flow, would help to more accurately characterize the complex frequency behavior of churn frequency.

An important observation regarding churn frequency is that the maximum churn frequency coincides with the point at which the total pressure gradient (evaluated as the difference in absolute pressure measured between 73.00*D* and 56.33*D*, divided by the distance between the two pressure transducers) becomes zero, as illustrated in Fig. 15. Given that the total pressure drop in vertical downward flow results from the balance between frictional and gravitational gradient pressure drop components, it can be observed that the transition from a gravity-dominated regime to one dominated by frictional effects is accompanied by an important change in the characteristic frequencies of churn flow.

To assess the impact of cap bubble, slug, and churn frequencies on the total pressure drop gradient, Fig. 16 presents the pressure gradient calculated from the second and third pressure transducers, plotted as a function of the estimated characteristic frequencies for each flow regime. For cap bubble flow, the data reveal a weak correlation between frequency and pressure drop, indicating that cap bubble frequency has limited influence on the total pressure gradient under the conditions investigated. In the case of slug flow, the results show a more scattered distribution, which complicates drawing a definitive conclusion. Nevertheless, a general decreasing trend of pressure drop gradient with increasing slug frequency can be observed, suggesting a potential inverse relationship. Depending on whether gravitational or frictional pressure drop dominates, the churn flow data segregate into two distinct clusters. In both cases, a linear decrease in total pressure drop is observed with increasing churn frequency.

Traditionally, slug frequency is expressed in dimensionless form using the gas-based Strouhal number (St_G) defined in Eq. (7). This number was proposed by Fossa et al. (2003) and subsequently adopted by several researchers (Kaji et al., 2009; Arabi et al., 2020). Following the methodology of Arabi et al. (2020) concerning sub-regimes of horizontal intermittent flow, we present in Fig. 17 the variation of St_G as a function of the mixture Froude number. The results reveal that the experimental data corresponding to cap bubble, slug, and churn flows occupy distinct zones. The boundaries separating the flow regimes are clearly identifiable, with transitions between cap bubble and slug flow, and between slug and churn flow, corresponding to St_G values of approximately 0.190 and 0.055, respectively. The resulting data clusters define a type of flow map known as a "space feature" (Arabi et al., 2024; Bouderbal et al., 2024). These space features serve as a valuable tool for identifying flow regimes based on output parameters, in this case, the characteristic frequency. Additional experimental data involving broader ranges of superficial velocities, pipe diameters, and working fluids would help validate and generalize these findings for wider operational conditions.

$$St_G = \frac{f_c D}{V_{SG}} \tag{7}$$

Numerous studies in the open literature have demonstrated that the dimensionless slug frequency, expressed via the gas-based Strouhal

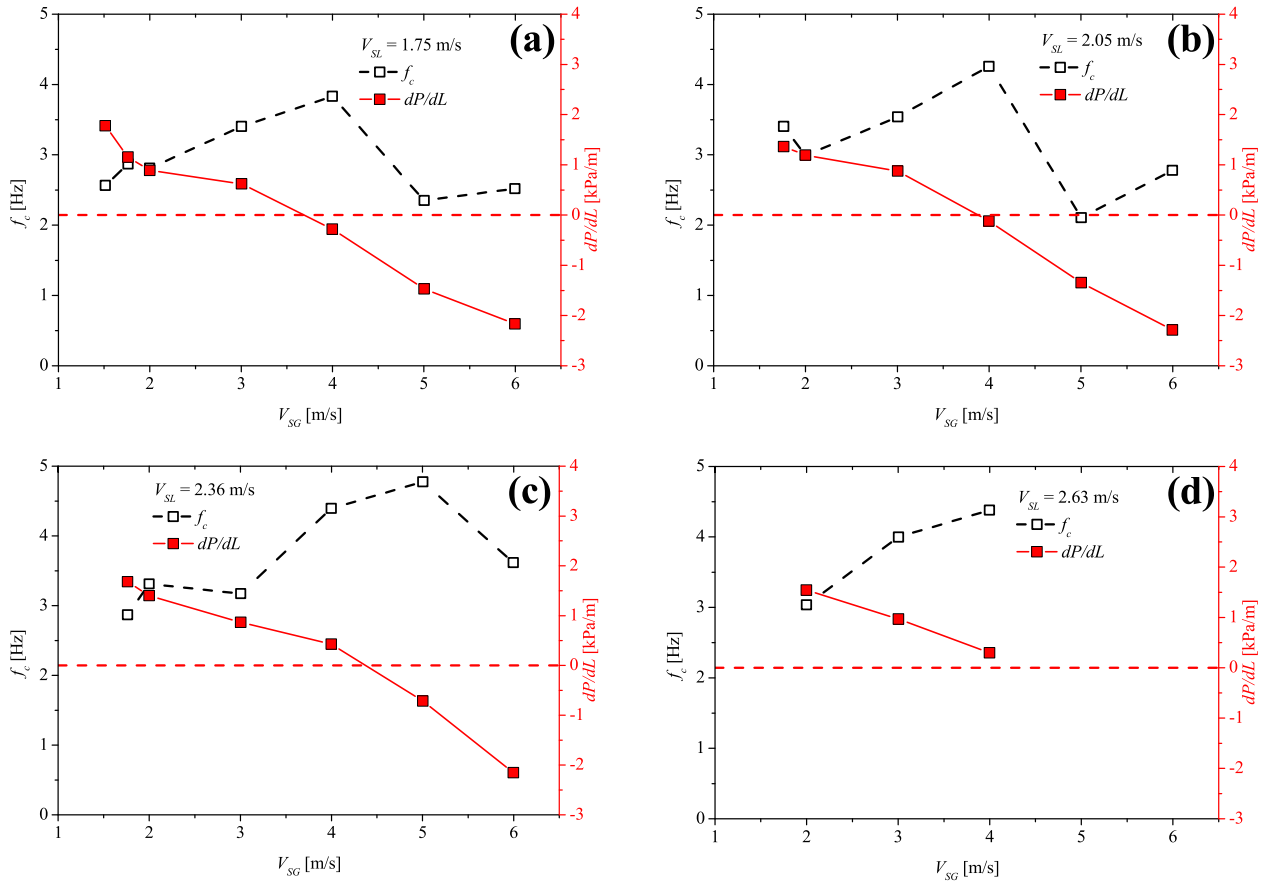

Fig. 15. Variation of churn frequencies and total pressure drop gradient with V_{SG} for different V_{SL}.

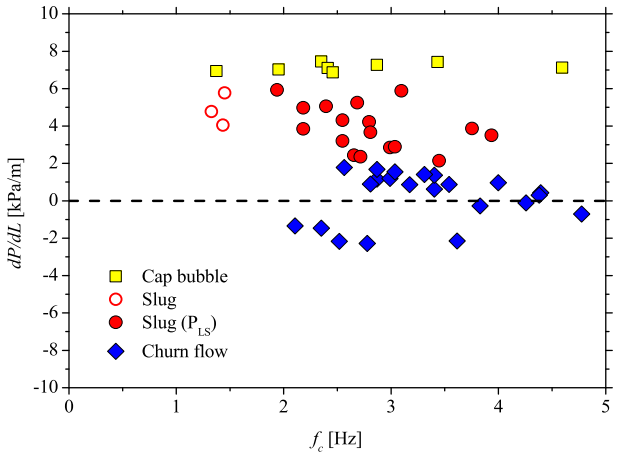

Fig. 16. Influence of characteristic frequencies on the total pressure drop gradient.

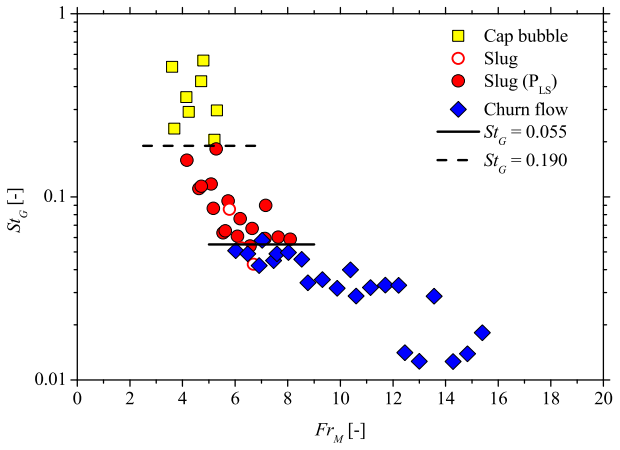

Fig. 17. Plot of the experimental characteristic frequencies using St_G vs Fr_M.

number, can be effectively correlated with the Lockhart–Martinelli parameter (X) given in Eq. (8). This relationship has been observed for different flow orientations, including horizontal flow (Azzi et al., 2010; Kong and Kim, 2021), vertical upward flow (Kaji et al., 2009; Waltrich et al., 2013), and vertical downward flow (Bouyahiaoui et al., 2018).

$$X = \sqrt{\frac{\left(\frac{dP}{dL}\right)_L}{\left(\frac{dP}{dL}\right)_G}} = \sqrt{\frac{\frac{f_L \rho_L V_{SL}^2}{2D}}{\frac{f_G \rho_G V_{SG}^2}{2D}}} = \sqrt{\frac{f_L \rho_L}{f_G \rho_G}} \frac{V_{SL}}{V_{SG}} \tag{8}$$

where $\left(\frac{dP}{dL}\right)_L$, $\left(\frac{dP}{dL}\right)_G$, f_L, f_G, ρ_L and ρ_G refer to the liquid frictional pressure drop, gas frictional pressure drop, liquid friction factor, gas friction factor, liquid and gas densities, respectively. The friction factors for the liquid and gas phases are calculated using Eq. (9). The correlation proposed by Fang et al. (2011) is adopted for turbulent flow conditions.

$$f_{L,G} = \begin{cases} \dfrac{64}{Re_{L,G}} \; if \; Re_{L,G} \leq 1050 \\ 0.25\left[log\left(\dfrac{150.39}{Re_{L,G}^{0.98865}} - \dfrac{152.66}{Re_{L,G}}\right)\right]^{-2} \; if \; Re_{L,G} > 1050 \end{cases} \tag{9}$$

The experimental data plotted in Fig. 18, along with those reported by Bouyahiaoui et al. (2018), reveal a clear linear alignment across the three observed flow regimes. It is noteworthy that the slug frequencies measured in the present study are higher than those obtained by Bouyahiaoui et al. (2018) for values of the Lockhart-Martinelli parameter $X < 50$. However, for higher X values, both datasets converge and exhibit similar trends.

3.5. Development of an intermittent characteristic frequency correlation

This section is dedicated to propose a new correlation for predicting the characteristic frequencies. The results presented in Figs. 17 and 18 clearly demonstrate that the gas-based Strouhal number is an effective non-dimensional parameter for representing cap bubble, slug, and churn frequencies in vertical downward flow. Building upon this observation, we adopted the St_G vs λ_L approach, previously applied with success in horizontal, and vertical upward orientations (Fossa et al., 2003; Arabi et al., 2020, 2022; Sassi et al., 2022; Cao et al., 2023, 2024; Rodrigues et al., 2025), to correlate the experimental results obtained in the present study.

In Fig. 19, the measured characteristic frequencies are plotted using the St_G vs λ_L representation. It can be observed that the data corresponding to cap bubble, slug, and churn flows in vertical downward orientation also align consistently, following a clear trend. In line with the approach proposed by Fossa et al. (2003), the following equation was adopted to correlate the experimental results:

$$St_G = \frac{a\lambda_L}{1 + b\lambda_L + c\lambda_L^2} \tag{10}$$

The coefficients a, b, and c were determined through nonlinear regression and found to be 0.1110, 2.3090, and −3.4015, respectively. The coefficient of determination (R^2) is equal to 96.28 %.

3.6. Assessment of predictive frequency models

The characteristic frequencies obtained from experiments were compared with both the newly proposed correlation and the model proposed by Bouyahiaoui et al. (2018). The performance of each correlation was assessed using notably two statistical performance indicators: the Average Absolute Relative Error (*AARE*) and the Average Relative Error (*ARE*). These metrics were calculated based on the Relative Error (*RE*) between the measured ($f_{c,mea}$) and calculated ($f_{c,cal}$) characteristic frequency values. The expressions for *RE*, *ARE*, and *AARE* are provided in Eqs. (12)–(14), respectively. In addition, the percentages of points predicted within ±10 %, ±20 %, ±25 %, and ±30 % error ranges were calculated. A summary of the performance indicators calculated for both models is presented in Table 4.

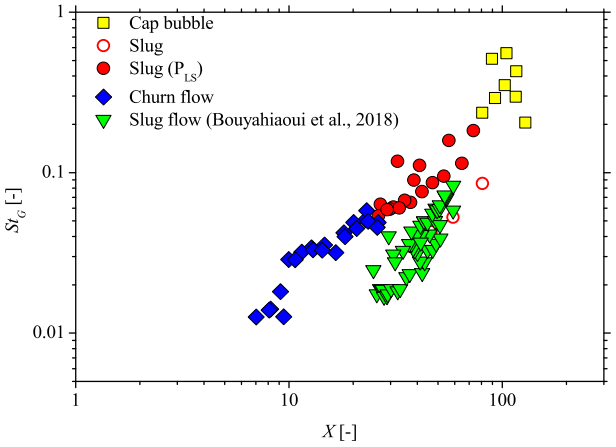

Fig. 18. Plot of the characteristic frequencies using St_G vs X.

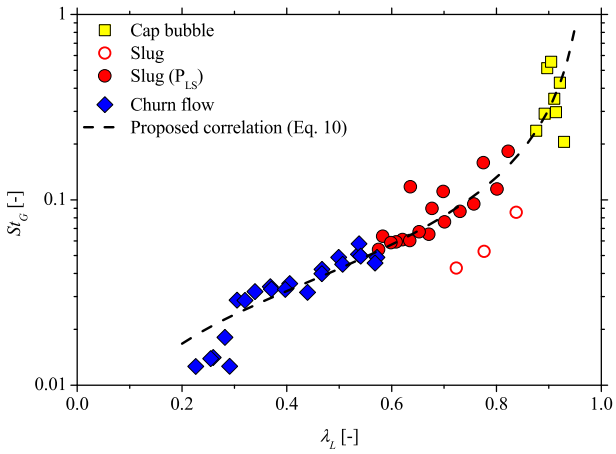

Fig. 19. Correlating the measured characteristic frequencies using St_G vs λ_L.

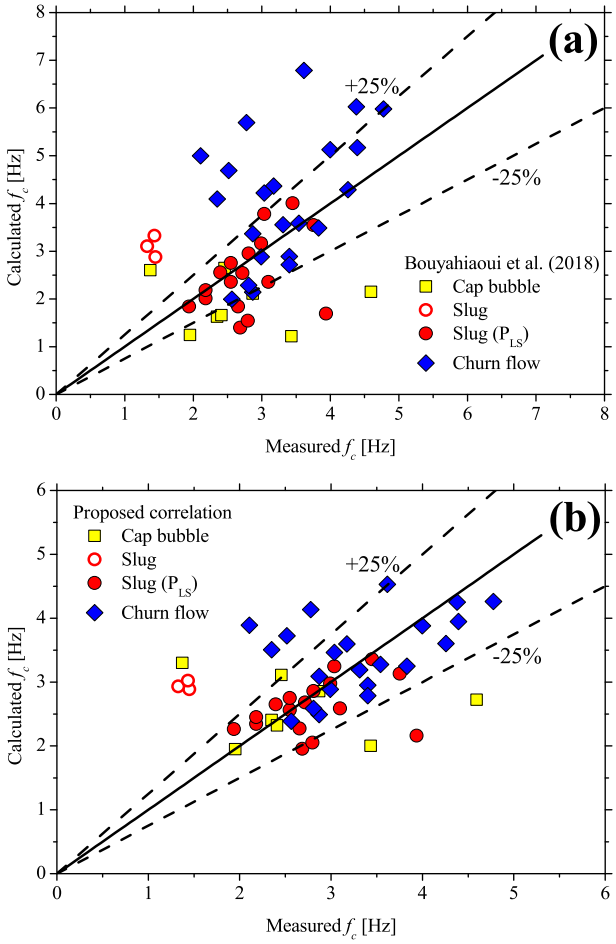

Fig. 20. Comparison of the measured characteristic frequencies with the prediction given by (a) the correlation of Bouyahiaoui et al. (2018), and (b) the proposed correlation.

Table 4
Prediction performance analysis of the evaluated correlation for predicting characteristic frequencies.

Performance indicators (%)	Bouyahiaoui et al. (2018)	Proposed correlation
ARE	−12.75	−9.75
AARE	36.46	24.49
Percentage of points predicted within ±10 % range	32.00	40.00
Percentage of points predicted within ±20 % range	42.00	70.00
Percentage of points predicted within ±25 % range	50.00	70.00
Percentage of points predicted within ±30 % range	58.00	78.00

$$RE = \frac{f_{c,mea} - f_{c,cal}}{f_{c,mea}} \times 100 \tag{12}$$

$$ARE = \sum_{i=1}^{N} RE \tag{13}$$

$$AARE = \sum_{i=1}^{N} |RE| \tag{14}$$

From Tables 4, it is evident that the proposed correlation provides the most accurate predictions, yielding the lowest values of both *ARE* and *AARE* (−9.75 % and 24.49 %, respectively). In addition, it predicts a higher number of data points within the ±10 %, ±20 %, ±25 %, and ±30 % error ranges.

To further evaluate the performance of the two correlations, comparative plots of predicted versus measured frequencies are provided in Fig. 20.a, respectively. As shown in Fig. 20.a, Bouyahiaoui et al.'s model provides reasonable predictions for slug flow, but underperforms for the P_{LS} sub-regime. This observation can be attributed to the fact that the study by Bouyahiaoui et al. (2018) focused exclusively on slug flow. Given the range of liquid superficial velocities investigated in their work (see Fig. 6, for instance), it is likely that the P_{LS} sub-regime was not encountered or reported. In contrast, Fig. 20.b clearly demonstrates that the proposed correlation performs well across all three flow regimes, cap bubble, slug, and churn. Therefore, the proposed model not only improves upon existing approaches but also offers broader applicability across intermittent flow regimes in vertical downward flow.

4. Conclusions

This study addresses the lack of experimental data and predictive models for the characteristic frequency of intermittent gas-liquid flows in vertical downward configurations. A total of 50 test conditions were explored using a 30 mm ID acrylic pipe and air-water mixture, with liquid superficial velocities ranging from 1.45 to 2.63 m/s. Characteristic frequencies were extracted from absolute pressure time series using the Welch method. The key findings can be summarized as follows:

1. High-speed imaging enabled detailed visualization of the flow structures, revealing three distinct flow regimes: cap bubble, slug, and churn flows. The analysis highlighted the presence of multi-scale structures and complex motion patterns within each regime. Based on these observations and analysis of forces acting on vertical downward flow, a new flow regime map was proposed using the modified Lockhart-Martinelli parameter and the mixture Froude number as coordinates.
2. Frequency measurements at three axial locations showed that characteristic frequencies increase along the flow development. In the present setup, the characteristic frequency stabilized at approximately 56.33D from the 90° bend.
3. The influence of superficial gas velocity on the characteristic frequency varied by flow regime. Cap bubble and slug frequencies generally increased with V_{SG}, whereas churn flow exhibited a non-monotonic trend, rising, then falling, and rising again, reflecting the complexity and multiple frequency components inherent in churn flow. Interestingly, the maximum churn frequency coincided with the transition from gravitational-dominated to frictional-dominated pressure drop.
4. The gas-based Strouhal number was successfully used to analyze and differentiate the flow regimes. A flow map based on St_G vs. Fr_M demonstrated distinct clustering of cap bubble, slug, and churn regimes, offering a practical space-feature tool for flow identification. Additionally, plotting St_G vs. X revealed a linear correlation across the three flow regimes investigated.
5. A new empirical correlation based on the St_G vs. λ_L approach was proposed. This correlation demonstrated superior accuracy compared to the existing model, particularly in capturing characteristic frequencies across all three flow regimes for the studied vertical downward configuration. Considering the fact that the proposed correlation was not validated with independent datasets, the generation of additional databases is strongly recommended.

CRediT authorship contribution statement

Abderraouf Arabi: Writing – original draft, Visualization, Validation, Software, Methodology, Investigation, Funding acquisition, Formal analysis, Data curation, Conceptualization. **Abdelhak Lakehal:** Writing – review & editing, Formal analysis. **Ronaldo Luis Höhn:** Writing – review & editing, Validation, Methodology. **Abdelwahid Azzi:** Writing – review & editing, Methodology. **Jordi Pallares:** Writing – review & editing, Visualization, Project administration, Funding acquisition. **Youssef Stiriba:** Writing – review & editing, Visualization, Project administration.

Declaration of generative AI and AI-assisted technologies in the writing process

During the preparation of this work the authors used OpenAI's ChatGPT-4o and ChatGPT-5 in order to enhance the language and clarity of this manuscript. After using this tool/service, the authors reviewed and edited the content as needed and take full responsibility for the content of the published article.

Declaration of competing interest

The authors declare that they have no known competing financial interests or personal relationships that could have appeared to influence the work reported in this paper.

Acknowledgements

A. A. has received funding from the Beatriu de Pinós postdoctoral fellowship program (2021 BP 00052) funded by the Secretary of Universities and Research of the government of Catalonia and the European Union's Horizon 2020 Program for Research and Innovation under Marie Skłodowska-Curie grant agreement No. 801370. This work was supported through project PID2023-146648NB-C21 funded by Spain's Ministerio de Ciencia e Innovación (MCIN) and Agencia Estatal de Investigación (AEI) and by project 2021SGR00732 of the Departament de Recerca i Universitats de la Generalitat de Catalunya. The authors appreciate the help of Daniel Graus Muñoz for the setup settings.

Appendix A. Supplementary data

Supplementary data related to this article can be found online at https://doi.org/10.1016/j.jgsce.2025.205827.

Data availability

Data will be made available on request.

References

Abdulkadir, M., Kajero, O.T., Olarinoye, F.O., Udebhulu, D.O., Zhao, D., Aliyu, A.M., Al-Sarkhi, A., 2021. Investigating the behaviour of air–water upward and downward flows: are you seeing what I am seeing? Energies 14 (21), 7071.

Abdul-Majeed, G., Al-Sarkhi, A., Al-Fatlawi, O.F., Mohmmed, A.O., 2025. Empirical model for predicting slug-pseudo slug and slug-churn transitions of upward air/water flow. Geoenergy Sci. Eng. 246, 213613.

Abdul-Majeed, G.H., Firouzi, M., Soto-Cortes, G., 2020. Prediction of slug frequency for medium liquid viscosity two-phase flow in vertical, horizontal, and inclined pipes. SPE Prod. Oper. 35 (4), 885–894.

Akhlaghi, M., Taherkhani, M., Nouri, N.M., 2020. Study of intermittent flow characteristics experimentally and numerically in a horizontal pipeline. J. Nat. Gas Sci. Eng. 79, 103326.

Al-Alweet, F.M., Almutairi, Z., Alothman, O.Y., Peng, Z., Alshammari, B.A., Almakhlafi, A., 2025. Time-dependent analysis of flow pattern developments in two-phase flow using capacitance sensors: fast fourier transform and total power spectrum exploration. Flow Meas. Instrum. 102, 102818.

Arabi, A., Höhn, R.L., Pallares, J., Stiriba, Y., 2025a. Practical aspects of multiphase slug frequency: an overview. Can. J. Chem. Eng. 103 (6), 2880–2894.

Arabi, A., Höhn, R.L., Pallares, J., Stiriba, Y., 2025b. New modeling approaches for liquid holdup and pressure drop in vertical downward gas-liquid two-phase flow. Int. J. Multiphas. Flow, 105371.

Arabi, A., Saidj, F., Al-Sarkhi, A., Azzi, A., 2022. Analogy between vertical upward cap bubble and horizontal plug flow. SPE J. 27 (3), 1577–1596.

Arabi, A., Salhi, Y., Zenati, Y., Si-Ahmed, E.K., Legrand, J., 2020. On gas-liquid intermittent flow in a horizontal pipe: influence of sub-regime on slug frequency. Chem. Eng. Sci. 211, 115251.

Arabi, A., Salhi, Y., Zenati, Y., Si-Ahmed, E.K., Legrand, J., 2024. Identifying the intermittent flow sub-regimes using pressure drop time series fluctuations. Experimental and Computational Multiphase Flow 6 (1), 28–40.

Arabi, A., Salhi, Y., Zenati, Y., Si-Ahmed, E.K., Legrand, J., 2025c. Analysis of horizontal gas-liquid intermittent flow subregime transitions: physical mechanisms and flow maps. Experimental and Computational Multiphase Flow 7 (1), 50–66.

Arellano, Y., Hunt, A., Haas, O., Ma, L., 2020. On the life and habits of gas-core slugs: characterisation of an intermittent horizontal two-phase flow. J. Nat. Gas Sci. Eng. 82, 103475.

Aursand, P., Hammer, M., Munkejord, S.T., Wilhelmsen, Ø., 2013. Pipeline transport of CO2 mixtures: models for transient simulation. Int. J. Greenh. Gas Control 15, 174–185.

Ayegba, P.O., Sebilleau, J., Colin, C., 2025. Modelling of wave velocity, wave frequency and interfacial friction factor in vertical upward and downward annular flow. Int. J. Heat Mass Tran. 247, 127157.

Azzi, A., Al-Attiyah, A., Qi, L., Cheema, W., Azzopardi, B.J., 2010. Gas–liquid two-phase flow division at a micro-T-junction. Chem. Eng. Sci. 65 (13), 3986–3993.

Bai, F., Jia, C., Hu, J., Alsousy, A., Lu, Y., Sepehrnoori, K., 2024. Storage capacity comparison of hydrogen and carbon dioxide in heterogeneous aquifers. Gas Sci. Eng. 121, 205182.

Bai, F., Lou, W., Lu, Y., 2023. A robust drift-flux model for two-phase CO2 pipe flow. Gas Sci. Eng. 119, 205140.

Barnea, D., Shoham, O., Taitel, Y., 1982. Flow pattern transition for vertical downward two phase flow. Chem. Eng. Sci. 37 (5), 741–744.

Bouderbal, A., Salhi, Y., Arabi, A., Si-Ahmed, E.K., Legrand, J., Arhaliass, A., 2024. Experimental investigation of different sub-regimes in horizontal stratified and intermittent gas-liquid two-phase flow: flow map and analysis of pressure drop fluctuations. Chem. Eng. Res. Des. 210, 407–424.

Boutaghane, A., Arabi, A., Ibrahim-Rassoul, N., Al-sarkhi, A., Azzi, A., 2023. Analysis, comparison, and discussion on the utilization of the existing slug liquid holdup models to predict the horizontal gas-liquid plug-to-slug flow transition. J. Energy Resour. Technol. 145 (7), 074501.

Bouyahiaoui, H., Azzi, A., Zeghloul, A., Hasan, A.H., Al-Sarkhi, A., Parsi, M., 2020. Vertical upward and downward churn flow: similarities and differences. J. Nat. Gas Sci. Eng. 73, 103080.

Bouyahiaoui, H., Azzi, A., Zeghloul, A., Hasan, A., Berrouk, A.S., 2018. Experimental investigation of a vertically downward two-phase air-water slug flow. J. Petrol. Sci. Eng. 162, 12–21.

Bouyahiaoui, H., Saidj, F., Arabi, A., Al-Sarkhi, A., Azzi, A., 2024. Vertically downward gas-liquid flow: void fraction and pressure drop. Int. J. Multiphas. Flow 172, 104711.

Cao, Y., Xu, Q., Liu, T., Yu, H., Huang, B., Guo, L., 2023. Experimental investigation on long hydrodynamic slugs in offshore pipeline. Ocean Eng. 289, 116136.

Cao, Y., Xu, Q., Yu, H., Huang, B., Liu, T., Guo, L., 2024. Influence of pipeline diameters and fluid properties on slug frequency in horizontal pipelines. Chem. Eng. Sci. 283, 119397.

Cavalli, S., Alves, R.F., Bassani, C.L., Neto, M.A.M., Sum, A.K., Morales, R.E., 2024. Modulation of slug flow characteristics observed in three-phase solid-liquid-gas flow measurements. Chem. Eng. Sci. 300, 120596.

Chinello, G., Arellano, Y., Span, R., van Putten, D., Abdulrahman, A., Joonaki, E., et al., 2024. Toward standardized measurement of CO2 transfer in the CCS chain. Nexus 1 (2).

Daubechies, I., 1992. Ten lectures on wavelets. CBMS-NSF Regional Conference Series in Applied Mathematics. Society for Industrial and Applied Mathematics, Philadelphia, PA, USA.

Fabre, J., Liné, A., 1992. Modeling of two-phase slug flow. Annu. Rev. Fluid Mech. 24 (1), 21–46.

Fang, X., Xu, Y., Zhou, Z., 2011. New correlations of single-phase friction factor for turbulent pipe flow and evaluation of existing single-phase friction factor correlations. Nucl. Eng. Des. 241 (3), 897–902.

Fossa, M., Guglielmini, G., Marchitto, A., 2003. Intermittent flow parameters from void fraction analysis. Flow Meas. Instrum. 14 (4–5), 161–168.

Garbin, V., Bothe, D., Brenn, G., Casciola, C.M., Colin, C., Marengo, M., et al., 2025. Bubbles and bubbly flows. Int. J. Multiphas. Flow, 105240.

Garcia, C., Pereyra, E., Sarica, C., Korelstein, L., 2023. An improved unified correlation for prediction of slug frequency in gas-liquid flow. In: ISAVFT International Conference on Multiphase Production Technology (Pp. ISAVFT-2023). ISAVFT.

Gregory, G.A., Scott, D.S., 1969. Correlation of liquid slug velocity and frequency in horizontal cocurrent gas-liquid slug flow. AIChE J. 15 (6), 933–935.

Hammer, M., Deng, H., Liu, L., Langsholt, M., Munkejord, S.T., 2021. Upward and downward two-phase flow of CO2 in a pipe: comparison between experimental data and model predictions. Int. J. Multiphas. Flow 138, 103590.

Henry, M., 2024. An ultra-precise Fast Fourier Transform. Measurement: Sensors 32, 101039.

Hernandez–Perez, V., Abdulkadir, M., Azzopardi, B., 2010a. Slugging frequency correlation for inclined gas-liquid flow. World Acad. Sci. Eng. Technol. Int. J. Chem. Mol. Eng. 4, 10–17.

Hernandez-Perez, V., Azzopardi, B.J., Kaji, R., Da Silva, Beyer, M., Hampel, U., 2010b. Wisp-like structures in vertical gas–liquid pipe flow revealed by wire mesh sensor studies. Int. J. Multiphas. Flow 36 (11–12), 908–915.

Heywood, N.I., Richardson, J.F., 1979. Slug flow of air—water mixtures in a horizontal pipe: determination of liquid holdup by γ-ray absorption. Chem. Eng. Sci. 34 (1), 17–30.

Hibiki, T., Goda, H., Kim, S., Ishii, M., Uhle, J., 2004. Structure of vertical downward bubbly flow. Int. J. Heat Mass Tran. 47 (8–9), 1847–1862.

Höhn, R.L., Arabi, A., Ballesta, S.V.V., Sassi, P.J., Pallarès, J., Stiriba, Y., 2025. Analysis of flow regimes and volumetric phase fraction of vertical upward gas–liquid–solid three-phase flow. Can. J. Chem. Eng. 103 (9), 4513–4539.

Höhn, R.L., Arabi, A., Stiriba, Y., Pallares, J., 2024. A review of the measurement of the multiphase slug frequency. Processes 12 (11), 2500.

Holagh, S.G., Ahmed, W.H., 2024. Critical review of vertical gas-liquid slug flow: an insight to better understand flow hydrodynamics' effect on heat and mass transfer characteristics. Int. J. Heat Mass Tran. 225, 125422.

Holagh, S.G., Ahmed, W.H., 2025. Unlocking the dynamics of complex instability mechanisms in developing gravity-driven slug flows. Int. J. Multiphas. Flow 188, 105230.

Ishii, M., Zuber, N., 1979. Drag coefficient and relative velocity in bubbly, droplet or particulate flows. AIChE J. 25 (5), 843–855.

Johansson, P.S., Yang, Z., Larrey, D., Belt, R., Liu, L., 2024. Multiple holdup equilibria and hydraulic gradients in stratified gas–liquid flows. Gas Sci. Eng. 131, 205461.

Kaji, R., Azzopardi, B.J., Lucas, D., 2009. Investigation of flow development of co-current gas–liquid vertical slug flow. Int. J. Multiphas. Flow 35 (4), 335–348.

Kong, R., Kim, S., 2021. Frequency of plug/slug bubbles in horizontal air-water two-phase flow. In: International Conference on Nuclear Engineering (Vol. 85253, P. V002T07A004). American Society of Mechanical Engineers.

Korelstein, L., Pereyra, E., 2023. Universal gas-liquid flow pattern map and its use on closure relationship selection. In: E3S Web of Conferences (Vol. 397, P. 01002). EDP Sciences.

Lee, J.Y., Ishii, M., Kim, N.S., 2008. Instantaneous and objective flow regime identification method for the vertical upward and downward co-current two-phase flow. Int. J. Heat Mass Tran. 51 (13–14), 3442–3459.

Legius, H.J.W.M., Van den Akker, H.E.A., Narumo, T., 1997. Measurements on wave propagation and bubble and slug velocities in cocurrent upward two-phase flow. Exp. Therm. Fluid Sci. 15 (3), 267–278.

Lu, C., Kong, R., Qiao, S., Larimer, J., Kim, S., Bajorek, S., et al., 2018. Frictional pressure drop analysis for horizontal and vertical air-water two-phase flows in different pipe sizes. Nucl. Eng. Des. 332, 147–161.

Martin, C.S., 1976. Vertically downward two-phase slug flow. J. Fluid Eng. 98 (4), 715–722.

Mohmmed, A.O., Al-Kayiem, H.H., Osman, A.B., 2021. Investigations on the slug two-phase flow in horizontal pipes: past, presents, and future directives. Chem. Eng. Sci. 238, 116611.

Mohmmed, A.O., Al-Kayiem, H.H., Arabi, A., 2025. Impact of slug length in gas–liquid two-phase flow on the structural stress characteristics of horizontal rigid pipelines. Can. J. Chem. Eng. 103 (10), 5124–5142.

Mori, K., Kaji, M., Sekoguchi, K., Sakane, M., Nakazatomi, M., Shimizu, H., 1996. Wave venation in downward gas-liquid two-phase flow (part I, time-spatial behavior chart of interface and analysis of main wave-vein). Heat Tran. Jpn. Res.: Co-sponsored by the Society of Chemical Engineers of Japan and the Heat Transfer Division of ASME 25 (8), 499–510.

Osundare, O.S., Elliott, A., Falcone, G., Lao, L., 2022. Gas-liquid flow regime maps for horizontal pipelines: predicting flow regimes using dimensionless parameter groups. Multiphas. Sci. Technol. 34 (4).

Peng, H., Xu, Z.D., Lu, H., Xi, D., Xia, Z., Yang, C., Wang, B., 2024. A review of underground transport infrastructure monitoring in CCS: technology and Engineering Practice. Process Saf. Environ. Prot. 190, 726–745.

Pereyra, E., Torres, C., Mohan, R., Gomez, L., Kouba, G., Shoham, O., 2012. A methodology and database to quantify the confidence level of methods for gas–liquid two-phase flow pattern prediction. Chem. Eng. Res. Des. 90 (4), 507–513.
Qiao, S., Li, J., Ren, J., Kim, S., 2022. Experimental investigation on effects of flow orientation on interfacial structure of air–water two-phase flow. Coatings 13 (1), 5.
Rodrigues, C.C., Maldonado, P.A., Garcia, G.D., dos Santos, E.N., Neto, M.A.M., Liné, A., Morales, R.E., 2025. 3D (2D space and time) experimental analysis of vertical slug flow–part 1: Air-Water. Int. J. Multiphas. Flow, 105386.
Saidj, F., Arabi, A., Bouyahiaoui, H., Azzi, A., Hasan, A.H., 2025. Slug void fraction in vertical downward gas–liquid two-phase flow. Phys. Fluids 37 (1), 013367.
Sarkodie, K., Fergusson-Rees, A., Asiedu, N.Y., 2023. Improved phase fraction measurement via non-intrusive optical sensing for vertical upward gas-liquid flow. Gas Sci. Eng. 114, 204948.
Sassi, P., Fernandez, G., Stiriba, Y., Pallares, J., 2022. Effect of solid particles on the slug frequency, bubble velocity and bubble length of intermittent gas–liquid two-phase flows in horizontal pipelines. Int. J. Multiphas. Flow 149, 103985.
Schmelter, S., Knotek, S., Olbrich, M., Fiebach, A., Bär, M., 2021. On the influence of inlet perturbations on slug dynamics in horizontal multiphase flow—a computational study. Metrologia 58 (1), 014003.
Sekoguchi, K., Mori, K., 1997. New development of experimental study on interfacial structure in gas-liquid two-phase flow. In: Proc. 4th World Conference on Exp. Heat Transf. Fluid Mech. Thermodyn, Brussels, pp. 1177–1188.
Sekoguchi, K., Mori, K., Kaji, M., Miwa, M., Nakazatomi, M., Shimizu, H., 1996a. Characteristics of interfacial profiles in upward and downward gas-liquid two-phase plug flow. Heat Tran. Jpn. Res. 25 (8), 568–579.
Sekoguchi, K., Mori, K., Kaji, M., Nakazatomi, M., Shimizu, H., 1996b. Interfacial profiles and flow characteristics in vertical downward two-phase plug and foam flows. Chem. Eng. Commun. 141 (1), 415–441.
Soedarmo, A.A., Rodrigues, H.T., Pereyra, E., Sarica, C., 2019. A new objective and distribution-based method to characterize pseudo-slug flow from wire-mesh-sensors (WMS) data. Exp. Therm. Fluid Sci. 109, 109855.
Soto-Cortes, G., 2014. Effects of High Oil Viscosity on Oil-Gas Behavior in Deviated Pipes, TUFFP 83rd Semi-annual Advisory Board Meeting. The University of Tulsa, Tulsa, OK, pp. 211–223, 2014.
Soto-Cortes, G., Pereyra, E., Sarica, C., Torres, C., Soedarmo, A., 2021a. Signal processing for slug flow analysis: MATLAB algorithm. MethodsX 8, 101546.
Soto-Cortes, G., Pereyra, E., Sarica, C., Torres, C., Soedarmo, A., 2021b. Signal processing for slug flow analysis via a voltage or instantaneous liquid holdup time-series. Flow Meas. Instrum. 79, 101968.
Usui, K., Sato, K., 1989. Vertically downward two-phase flow, (I) void distribution and average void fraction. J. Nucl. Sci. Technol. 26 (7), 670–680.
van Hout, R., Shemer, L., Barnea, D., 2003. Evolution of hydrodynamic and statistical parameters of gas–liquid slug flow along inclined pipes. Chem. Eng. Sci. 58 (1), 115–133.
Vaziri, P., Rasaei, M.R., Seyfoori, S., Zamani, S., Mahmoodi, M., Sedaee, B., 2024. Advancing carbon capture technologies in CCS: a comprehensive review of pre-combustion processes. Gas Sci. Eng., 205481
Waltrich, P.J., Falcone, G., Barbosa Jr, J.R., 2013. Axial development of annular, churn and slug flows in a long vertical tube. Int. J. Multiphas. Flow 57, 38–48.
Wu, B., Firouzi, M., Mitchell, T., Rufford, T.E., Leonardi, C., Towler, B., 2017. A critical review of flow maps for gas-liquid flows in vertical pipes and annuli. Chem. Eng. J. 326, 350–377.
Zadrazil, I., Matar, O.K., Markides, C.N., 2014. An experimental characterization of downwards gas–liquid annular flow by laser-induced fluorescence: Flow regimes and film statistics. Int. J. Multiphas. Flow 60, 87–102.
Zhai, L., Zhong, X., Meng, X., Pu, G., Jin, N., 2025. Mechanism of slug aeration in horizontal gas-liquid intermittent flow: insights from S-PLIF and PIV analysis. Chem. Eng. J. 505, 159089.